Phases of ^{3}He-^{4}He mixtures in two dimensions

E. Krotscheck,[1] J. Paaso,[2] M. Saarela,[2] and K. Schörkhuber[1]
[1]*Institut für Theoretische Physik, Johannes Kepler Universität, A 4040 Linz, Austria*
[2]*Physical Sciences/Theoretical Physics, P.O. Box 3000, FIN-90014 University of Oulu, Finland*
(Received 10 November 2000; published 3 July 2001)

We calculate the phase diagram of ^{3}He-^{4}He mixtures in two dimensions as a function of density and ^{3}He concentration. A number of features distinguish this system significantly from its three-dimensional counterpart. Specifically, we find that the ^{3}He phase consists, at low ^{3}He concentrations and positive pressures, of loosely bound dimers. The dimerized liquid phase separates at a ^{3}He concentration of 2–3 % because the chemical potential of the ^{3}He component in the mixture exceeds the chemical potential in the pure phase. Atomic ^{3}He-^{4}He mixtures can be found only in a metastable state in a concentration regime above 3%, where the mixture is stable against infinitesimal concentration fluctuations. The softening of concentration-fluctuation modes with decreasing ^{3}He concentration is accompanied by a divergence of the ^{3}He hydrodynamic effective mass, and the magnetic susceptibility vanishes. We verify, wherever possible, that our results are consistent with simulation data and exact estimates.

DOI: 10.1103/PhysRevB.64.054504 PACS number(s): 67.60.−g, 67.57.Pq, 68.15.+e, 68.35.Rh

I. INTRODUCTION

Two-dimensional mixtures of the quantum liquids ^{3}He and ^{4}He can, under certain circumstances, serve as models for atomic monolayers of ^{3}He and ^{4}He on strongly attractive substrates. These systems have drawn much theoretical and experimental attention during the past two decades.[1–4] Our paper describes a systematic application of modern many-body technology to this family of physical systems. We shall see that the two-dimensional mixture is in many aspects quite dis-similar to its three-dimensional counterpart, in particular we find that, at zero temperature, the only stable phase is a mixture of very loosely bound ^{3}He *dimers* within a ^{4}He host liquid.[5]

We utilize for our studies the optimized variational theory described in detail in Ref. 6. This method has been applied extensively to homogeneous and inhomogeneous bosonic quantum liquids and liquid mixtures, reaching agreement with simulation data or experiments at the percent level or better. The theory has been reviewed extensively, there is, therefore, no need to describe the theoretical tools in detail. Instead, we shall only mention in the next section the basic steps necessary for the implementation of the theory, and highlight only those aspects and relationships that are important for the discussion of its physical content.

We then turn to the application of the theory, and, along with that, a step-by-step verification of our results with simulation data where available. Two calculations are presented: We first calculate the properties of *single* ^{3}He atoms in the host liquid, as well as the effective interactions between *pairs* of ^{3}He atoms. We show that this effective interaction is sufficiently attractive to cause a loosely bound dimer of ^{3}He atoms. We then study the properties and the stability of the mixture at finite concentrations of ^{3}He. The actual calculation then shows that a locally stable homogeneous mixture can exist only *above* a concentration of a few percent. Global energy considerations then show that this phase is unstable against *macroscopic* concentration fluctuations.

We finally discuss the ramifications of our findings for the nature of monolayer mixture films. Among others, we calculate the dynamic structure function in a simple approximation, and compute the effective mass and the magnetic susceptibility of the ^{3}He component.

II. VARIATIONAL THEORY AND CORRELATED-BASIS FUNCTIONS

Many ground-state properties of ^{3}He-^{4}He mixtures, in particular the energetics of the system and the local structure, are today quite well understood both experimentally[7] and theoretically from a microscopic point of view[6] in three dimensions. With ''microscopic'' we mean that one postulates no more knowledge than the empirical Hamiltonian

$$H=-\sum_{\alpha}\sum_{i=1}^{N_\alpha}\frac{\hbar^2}{2m_\alpha}\nabla_i^2+\frac{1}{2}\sum_{\alpha,\beta}{\sum_{i,j}}'^{N_\alpha,N_\beta} V^{(\alpha\beta)}(|\mathbf{r}_i-\mathbf{r}_j|) \tag{2.1}$$

that contains only a local two-body interaction; recent work uses most frequent versions of the Aziz interaction.[8,9]

To specify our notation we use in the following Greek subscripts $\alpha,\beta,\ldots\in\{3,4\}$ to refer to the *particle species* (a ^{3}He or a ^{4}He particle), and Latin subscripts $i,j,\ldots$ as in the $\mathbf{r}_i$ to refer to the individual particles. The prime on the summation symbol in Eq. (2.1) indicates that no two pairs (i,α), (j,β) can be the same. The number of particles of each species is N_α, and $N=N_3+N_4$ is the total number of particles in the system. In terms of the ^{3}He concentration x we have

$$N_3=xN,\quad N_4=(1-x)N, \tag{2.2}$$

and the corresponding partial densities,

$$\rho_3=x\rho,\quad \rho_4=(1-x)\rho, \tag{2.3}$$

are proportional to the total number density $\rho=N/\Omega$, where Ω is the volume occupied by the whole fluid.

The Jastrow-Feenberg variational method[10,11] and its extensions within the theory of correlated-basis functions[10] (CBF) provides the necessary tools for a precise ground-state calculation. When applied to fermions, two steps are essential that we shall describe briefly below. These are (i) the construction and optimization of a suitable variational wave function, and (ii) the improvement of the description of the system by CBF perturbation theory.

A. Optimized variational wave functions

We start with a variational ansatz for the ground-state wave function that incorporates both pair and triplet-correlation functions in the form

$$\Psi_0(\{\mathbf{r}_i^{(\alpha)}\}) = \exp\left[\frac{1}{2}U(\{\mathbf{r}_i^{(\alpha)}\})\right]\Phi_0(\{\mathbf{r}_i^{(3)}\}),$$

$$U(\{\mathbf{r}_i^{(\alpha)}\}) = \frac{1}{2!}\sum_{\alpha\beta}\sum_{i,j}^{N_\alpha,N_\beta}{}' u^{(\alpha\beta)}(\mathbf{r}_i,\mathbf{r}_j) + \frac{1}{3!}\sum_{\alpha\beta\gamma}\sum_{i,j,k}^{N_\alpha,N_\beta,N_\gamma}{}' u^{(\alpha\beta\gamma)}(\mathbf{r}_i,\mathbf{r}_j,\mathbf{r}_k). \tag{2.4}$$

Here $\Phi_0(\{\mathbf{r}_i^{(3)}\})$ is the Slater determinant of plane waves ensuring the antisymmetry of the fermion component of the wave function. The functions $u^{(\alpha\beta)}(\mathbf{r}_i,\mathbf{r}_j)$ and $u^{(\alpha\beta\gamma)}(\mathbf{r}_i,\mathbf{r}_j,\mathbf{r}_k)$ are the pair and triplet correlations; the species superscripts determine the type of correlation. An essential part of the method is the optimization of the ground-state correlations by the variational principles[12–14]

$$\frac{\delta E_0}{\delta u^{(\alpha\beta)}(\mathbf{r}_i,\mathbf{r}_j)} = 0, \quad \frac{\delta E_0}{\delta u^{(\alpha\beta\gamma)}(\mathbf{r}_i,\mathbf{r}_j,\mathbf{r}_k)} = 0, \tag{2.5}$$

where

$$E_0 = \frac{\langle\Psi_0|H|\Psi_0\rangle}{\langle\Psi_0|\Psi_0\rangle} \tag{2.6}$$

is the variational energy expectation value. Details of the procedure, and the necessary working formulas, have been discussed in Ref. 6. In particular the treatment of triplet correlations and elementary diagrams is a reasonably unpleasant task that provides little physical insight. We shall therefore restrict the discussion to pair correlations and only point out the modifications and corrections introduced by triplet correlations where appropriate.

The key ingredients of the theory are the correlation functions $u^{(\alpha\beta)}(\mathbf{r}_i,\mathbf{r}_j)$, the partial densities ρ_α, and the pair distribution functions

$$\rho_\alpha\rho_\beta g^{(\alpha\beta)}(r) \equiv \rho_\alpha\rho_\beta g^{(\alpha\beta)}(|\mathbf{r}-\mathbf{r}'|) = \sum_{i,j}^{N_\alpha,N_\beta}{}' \frac{\langle\Psi_0|\,\delta(\mathbf{r}_i^{(\alpha)}-\mathbf{r})\,\delta(\mathbf{r}_j^{(\beta)}-\mathbf{r}')|\Psi_0\rangle}{\langle\Psi_0|\Psi_0\rangle}. \tag{2.7}$$

Related to the pair-distribution functions are the static-structure functions

$$S^{(\alpha\beta)}(k) = \delta_{\alpha\beta} + \sqrt{\rho_\alpha\rho_\beta}\int d^2r[g^{(\alpha\beta)}(r)-1]e^{i\mathbf{r}\cdot\mathbf{k}}. \tag{2.8}$$

Relationships between the correlation functions $u^{(\alpha\beta)}(\mathbf{r}_i,\mathbf{r}_j)$ and the distribution functions $g^{(\alpha\beta)}(\mathbf{r}_i,\mathbf{r}_j)$ are provided by the (Fermi) hypernetted-chain [(F)HNC] hierarchy of integral equations. We are interested in ^{3}He-^{4}He mixtures with a dilute ^{3}He component. The closest where this can be achieved experimentally are atomic monolayers. For such low concentrations, the simplest version of the FHNC equations,[15,16] dubbed FHNC//0, is adequate to describe the correlations between the ^{3}He particles. This version of the FHNC theory sums self-consistently all chain and parallel-connected diagrams, but omits propagator corrections that have some quantitative effects[17] in pure ^{3}He. Practical implementations of the Euler equations (2.5) use the (F)HNC relationships to eliminate the correlation functions and to express the Euler equations entirely in terms of the physically observable distribution- and structure functions.

For mixtures, it is convenient to introduce a matrix notation, for example,

$$\mathbf{S}(k) \equiv [S^{(\alpha\beta)}(k)] \tag{2.9}$$

for the static structure functions. The static structure function of the *noninteracting* mixture has only a nontrivial (33) component,

$$\mathbf{S_F}(k) \equiv \begin{pmatrix} S_F(k) & 0 \\ 0 & 1 \end{pmatrix}, \tag{2.10}$$

where $S_F(k)$ is the static structure function of the noninteracting Fermi system,

$$S_F(k) = \begin{cases} \frac{2}{\pi}(\arcsin x + x\sqrt{1-x^2}) & \text{if } x \equiv k/2k_F < 1 \\ 1 \quad \text{otherwise.} \end{cases} \tag{2.11}$$

For further reference, we also need the matrix of ''dressed'' correlation functions $\tilde{\mathbf{\Gamma}}(k) = [\tilde{\Gamma}^{(\alpha\beta)}(k)]$ that is related to the structure-function matrix by

$$\mathbf{S}(k) = \mathbf{S_F}(k) + \mathbf{S_F}(k)\tilde{\mathbf{\Gamma}}(k)\mathbf{S_F}(k). \tag{2.12}$$

Generally, we use the tilde notation for the dimensionless Fourier transform, i.e.,

$$\tilde{f}^{(\alpha\beta)}(k) \equiv \sqrt{\rho_\alpha\rho_\beta}\int d^2r f^{(\alpha\beta)}(r)e^{i\mathbf{r}\cdot\mathbf{k}}. \tag{2.13}$$

Without going into further details of the derivations, we assert that the coupled Euler equations (2.5) for the $u^{(\alpha\beta)}(r)$ are equivalent to[6]

$$[\mathbf{S}^{-1}\mathbf{H_1}\mathbf{S}^{-1}](k) - [\mathbf{S_F}^{-1}\mathbf{H_1}\mathbf{S_F}^{-1}](k) = 2\tilde{\mathbf{V}}_{\text{p-h}}(k), \tag{2.14}$$

where

$$\mathbf{H_1}(k) \equiv \begin{pmatrix} \frac{\hbar^2 k^2}{2m_3} & 0 \\ 0 & \frac{\hbar^2 k^2}{2m_4} \end{pmatrix} \equiv \begin{pmatrix} t_3(k) & 0 \\ 0 & t_4(k) \end{pmatrix} \quad (2.15)$$

is the kinetic energy matrix, and

$$\tilde{\mathbf{V}}_{\text{p-h}}(k) \equiv [\tilde{V}_{\text{p-h}}^{(\alpha\beta)}(k)] \quad (2.16)$$

is the so-called *particle-hole interaction.* $\tilde{\mathbf{V}}_{\text{p-h}}(k)$ has the coordinate space form

$$V_{\text{p-h}}^{(\alpha\beta)}(r) = [1+\Gamma^{(\alpha\beta)}(r)][V^{(\alpha\beta)}(r)+\Delta V^{(\alpha\beta)}(r)] + \left[\frac{\hbar^2}{2m_\alpha}+\frac{\hbar^2}{2m_\beta}\right]|\nabla\sqrt{1+\Gamma^{(\alpha\beta)}(r)}|^2 + \Gamma^{(\alpha\beta)}(r) w_{\text{I}}^{(\alpha\beta)}(r). \quad (2.17)$$

Equation (2.17) defines a *static,* effective interaction $V_{\text{p-h}}^{(\alpha\beta)}(r)$. The quantities $\Delta V^{(\alpha\beta)}(r)$ are corrections due to elementary diagrams and triplet correlations; they must be calculated individually and are, in this sense, an external input to the theory. The ''induced interaction'' is

$$\tilde{\mathbf{w}}_{\text{I}}(k) = -\tilde{\mathbf{V}}_{\text{p-h}}(k) - \frac{1}{2}[\mathbf{S_F}^{-1}\mathbf{H_1}\tilde{\mathbf{\Gamma}} + \tilde{\mathbf{\Gamma}}\mathbf{H_1}\mathbf{S_F}^{-1}](k). \quad (2.18)$$

Equation (2.14) is known as the PPA equation from its first derivation by the ''paired-phonon analysis.[11]'' For any given choice of elementary diagrams and three-body correlations, the equations (2.14), (2.17), and (2.18) form a closed set of equations that can be solved by iteration until convergence is reached. Given the resulting distribution- and structure-functions, the variational energy expectation value (2.6) is then calculated as described in Ref. 6.

For reference, and also for discussing one of the key messages of this paper, we also display the coordinate-space form of the Euler equations (2.14) and (2.18). Adding the particle-hole interaction $\tilde{\mathbf{V}}_{\text{p-h}}(k)$ to both sides of Eq. (2.18), we obtain

$$-\frac{1}{2}[\mathbf{S_F}^{-1}\mathbf{H_1}\tilde{\mathbf{\Gamma}} + \tilde{\mathbf{\Gamma}}\mathbf{H_1}\mathbf{S_F}^{-1}](k) = \tilde{\mathbf{V}}_{\text{p-h}}(k) + \tilde{\mathbf{w}}_{\text{I}}(k). \quad (2.19)$$

If the $\mathbf{S_F}^{-1}$ were absent on the left-hand side of Eq. (2.19), we could rewrite it in coordinate space in the form of an effective Schrödinger equation for $\sqrt{1+\Gamma^{(\alpha\beta)}(r)}$,

$$\left(\frac{\hbar^2}{2m_\alpha}+\frac{\hbar^2}{2m_\beta}\right)\nabla^2\sqrt{1+\Gamma^{(\alpha\beta)}(r)} = [V(r)+\Delta V^{(\alpha\beta)}(r)+w_{\text{I}}^{(\alpha\beta)}(r)]\sqrt{1+\Gamma^{(\alpha\beta)}(r)}. \quad (2.20)$$

While such a Schrödinger-type equation for the determination of the short-range behavior of the correlations is naively plausible, we point out that the short-range structure of the wave function is determined by the Bethe-Goldstone equation, which differs from the Schrödinger equation by the appearance of Pauli-projection operators in the intermediate states. These are, within the variational framework, manifested by the factors $\mathbf{S_F}^{-1}$ in Eq. (2.19).

B. Correlated-basis functions

The Jastrow-Feenberg theory for *bosons* is a systematic method that leads, in principle, to the exact-wave function. The same is not the case for a Fermi system. The most apparent reason for this is that the wave function (2.4) has the nodes of the wave function of the free Fermi gas; but there is no reason that the exact-wave function should have the same nodes. This is so far an observation, but it makes no statement on how interactions move the nodes of the many-body wave function. This information is provided by comparing the results of the Jastrow-Feenberg variational theory with what perturbation theory would predict. The bottom-line conclusion is that the Jastrow-Feenberg function (2.4) replaces the particle-hole propagator by a ''collective'' or ''mean spherical'' approximation (MSA).[18,19] This is already seen in the weakly interacting limit and has, among others, the consequence that the wave function (2.4) does not reproduce the correct high-energy limit of the correlation energy of the electron gas. It also has consequences for the stability of the mixture, which we will discuss below.

The formally systematic way to go beyond the Jastrow-Feenberg theory is CBF theory.[10,20] The theory extends the use of the correlation operator $\exp[\frac{1}{2}U(\{\mathbf{r}_i^{(\alpha)}\})]$ to generate a nonorthogonal basis of the Hilbert space

$$|\Psi_{\mathbf{m}}\rangle = \mathrm{I}_{\mathbf{mm}}^{-1/2}\exp\left[\frac{1}{2}U(\{\mathbf{r}_i^{(\alpha)}\})\right]|\Phi_{\mathbf{m}}\rangle, \quad (2.21)$$

$$\mathrm{I}_{\mathbf{mm}} = \langle\Phi_{\mathbf{m}}|\exp[U(\{\mathbf{r}_i^{(\alpha)}\})]|\Phi_{\mathbf{m}}\rangle, \quad (2.22)$$

where $\{|\Phi_{\mathbf{m}}\rangle\}$ is a complete set of Slater determinants. The purpose of CBF theory is, in our context, to relax the ''mean spherical'' approximation for the particle-hole propagator. The relationship to the variational and CBF theory is not immediately obvious, and the actual calculations are quite tedious since they require both an (F)HNC analysis[21] of the effective interactions defined by CBF theory and an analysis of ring diagrams in correlated-basis functions[22] to all orders. Nevertheless, the result is quite plausible: The effect of summing all ring diagrams in CBF theory is simply to remove the collective approximation, in other words one obtains an energy correction

$$\Delta E_{\text{RPA}} = E_{\text{RPA}} - E_{\text{RPA}}^{\text{MSA}} = \frac{1}{2\rho}\,\mathrm{Im}\int\frac{d^2k\,d(\hbar\omega)}{(2\pi)^3}\ln[D(k,\omega)/D^{\text{MSA}}(k,\omega)], \quad (2.23)$$

where

$$D(k,\omega) = [1-\chi_0^{(33)}(k,\omega)\tilde{V}_{\text{p-h}}^{(33)}(k)][1-\chi_0^{(44)}(k,\omega)\tilde{V}_{\text{p-h}}^{(44)}(k)] - \chi_0^{(33)}(k,\omega)\chi_0^{(44)}(k,\omega)[\tilde{V}_{\text{p-h}}^{(34)}(k)]^2. \quad (2.24)$$

Here $\chi_0^{(33)}(k,\omega)$ is the Lindhard function, and $\chi_0^{(44)}(k,\omega)$ the response function of the noninteracting Bose system

$$\chi_0^{(44)}(k,\omega)=\frac{2t_4(k)}{(\hbar\omega+i\eta)^2-t_4^2(k)}. \tag{2.25}$$

$D^{\mathrm{MSA}}(k,\omega)$ is the same as expression (2.24), where the Lindhard function $\chi_0^{(33)}(k,\omega)$ is replaced by the ''mean-spherical approximation''

$$\chi_{0,\mathrm{MSA}}^{(33)}(k,\omega)=\frac{2t_3(k)}{(\hbar\omega+i\eta)^2-\hbar^2\omega_3^2(k)}, \tag{2.26}$$

where

$$\hbar\omega_3(k)\equiv t_3(k)/S_F(k) \tag{2.27}$$

is an effective collective energy, determined such that the $\chi_{0,\mathrm{MSA}}^{(33)}$ satisfies the first two energy-weighted sum rules. The same corrections are also introduced in the (F)HNC-EL (Euler-Lagrange) equations as described in detail in Ref. 6; the effect of introducing CBF corrections to infinite order is that the PPA equation (2.14) is replaced by an ordinary random-phase approximation (RPA) equation.[23] In the mixture, the density-density response function is a 2×2 matrix, which is given, in the RPA, by

$$\boldsymbol{\chi}(k,\omega)=\boldsymbol{\chi}_0(k,\omega)+\boldsymbol{\chi}_0(k,\omega)\tilde{\mathbf{V}}_{\text{p-h}}(k)\boldsymbol{\chi}(k,\omega), \tag{2.28}$$

where

$$\boldsymbol{\chi}_0(k,\omega)=\begin{pmatrix}\chi_0^{(33)}(k,\omega) & 0\\ 0 & \chi_0^{(44)}(k,\omega)\end{pmatrix}. \tag{2.29}$$

The static structure function is then calculated from the dynamic structure function

$$\mathbf{S}(k,\omega)=-\frac{1}{\pi}\mathrm{Im}\,\boldsymbol{\chi}(k,\omega), \tag{2.30}$$

through the fluctuation-dissipation theorem

$$\mathbf{S}(k)=\int_0^\infty d(\hbar\omega)\mathbf{S}(k,\omega). \tag{2.31}$$

Using the ''mean-spherical approximation'' $\chi_{0,\mathrm{MSA}}^{(33)}(k,\omega)$ instead of the Lindhard function in Eq. (2.28) leads immediately to the Euler equation (2.14) of the (F)HNC-EL theory. We shall return to the issues raised by CBF theory in the next section, when it comes to the interpretation of effective interactions.

III. SINGLE-IMPURITY AND TWO-IMPURITY LIMITS

It is instructive for the analysis of mixtures to study also its low-concentration limit, to examine the properties of only one impurity, and to calculate the effective interactions between isolated pairs of impurities. The calculation can be carried out in two ways: The normal approach is to start again with a variational wave for the system with one or two impurities, and to develop the Euler-Lagrange theory for this case. This method provides operational definitions of the basic ingredients. Alternatively, one may start from the mixture equations, and expand these equations to first and second order in the concentration x. We shall follow this route because it also gives us the freedom to consider the case that the impurities are a dilute gas of weakly correlated fermions at low density. In any case, we need to review the definitions of the basic ingredients of the theory, point out their physical interpretation, and highlight cases where the definitions deviate from those of the mixture theory.

In the limit that we have only one ^{3}He atom in the fluid of ^{4}He particles, the wave function is obtained from the mixture wave function by omitting all correlation functions containing two or more ^{3}He indices, and by setting the Slater determinant equal to one. As a convention we denote in this section the impurity coordinate with $\mathbf{r}_0$, in distinction from the ^{4}He particle coordinates $\mathbf{r}_i$ where $1\leqslant i\leqslant N_4\equiv N$. The wave function of the impurity plus background system is

$$\begin{aligned}\Psi_{N+1}^I(\mathbf{r}_0,\mathbf{r}_1,\ldots,\mathbf{r}_N)&=\exp\frac{1}{2}\Bigg[\sum_{j=1}^N u^{(34)}(\mathbf{r}_0,\mathbf{r}_j)+\frac{1}{2!}\sum_{i,j=1}^{N}{}' u^{(44)}(\mathbf{r}_i,\mathbf{r}_j)\\&+\frac{1}{2!}\sum_{i,j=1}^{N}{}' u^{(344)}(\mathbf{r}_0,\mathbf{r}_j,\mathbf{r}_k)\\&+\frac{1}{3!}\sum_{i,j,k=1}^{N}{}' u^{(444)}(\mathbf{r}_i,\mathbf{r}_j,\mathbf{r}_k)\Bigg],\end{aligned} \tag{3.1}$$

and its chemical potential

$$\mu_3=\frac{\langle\Psi_{N+1}^I|H_{N+1}^I|\Psi_{N+1}^I\rangle}{\langle\Psi_{N+1}^I|\Psi_{N+1}^I\rangle}-\frac{\langle\Psi_N|H_N|\Psi_N\rangle}{\langle\Psi_N|\Psi_N\rangle}\equiv E_{N+1}^I-E_N. \tag{3.2}$$

Here, H_N is the Hamiltonian of the N-particle background liquid, and H_{N+1}^I the Hamiltonian of the $(N+1)$-particle system consisting of N ^{4}He background atoms and one impurity.

The impurity correlations are again determined by the variational principle. Since the background energy does not depend on the impurity concentration, the Euler equation for the impurity correlations is equivalent to minimizing the chemical potential

$$\frac{\delta\mu_3}{\delta u^{(34)}(\mathbf{r}_0,\mathbf{r}_1)}=0,\quad \frac{\delta\mu_3}{\delta u^{(344)}(\mathbf{r}_0,\mathbf{r}_1,\mathbf{r}_2)}=0. \tag{3.3}$$

The impurity structure function is calculated from the pair-distribution function as

$$S^{(34)}(k)=\rho_4\int d^2r e^{i\mathbf{k}\cdot\mathbf{r}}[g^{(34)}(r)-g^{(34)}(\infty)]. \tag{3.4}$$

Note that the normalization factor of the impurity structure function is ρ_4 and not $\sqrt{\rho_3\rho_4}$ as in the mixture case. The value of the impurity structure function at the origin is the volume excess factor,[24]

$$S^{(34)}(0+)=-\beta. \tag{3.5}$$

The two-body Euler equations for the single impurity can be obtained directly from the mixture Euler equations (2.14) by setting $S_F(k)=S^{(33)}(k)=g^{(33)}(r)=1$,

$$\Gamma^{(\alpha\beta)}(r)=g^{(\alpha\beta)}(r)-1, \tag{3.6}$$

and observing the above change in normalization. For the purpose of our analysis we prefer, however, to be slightly more flexible and allow for a dilute gas of weakly correlated fermions. The low-concentration limit of Eqs. (2.14) and (2.18) is then taken such that all quantities contain no more than one (or two for the two-impurity case) dynamical impurity correlations, but they may still be correlated statistically to arbitrary orders. This implies, among others, that $S^{(34)}(k)=S_F(k)\tilde{\Gamma}^{(34)}(k)$. The rigorous single-impurity limit is then obtained by setting $S_F(k)=1$.

To see how this works, we start from the mixture Euler equation (2.14). The single-impurity limit implies that there cannot be two ^{3}He atoms dynamically correlated, hence we can set $\Gamma^{(33)}(k)=0$ and $S^{(33)}(k)=S_F(k)$. The (34)-channel equation then reads explicitly

$$\tilde{\Gamma}^{(34)}(k)=-2\frac{\tilde{V}^{(34)}_{\text{p-h}}(k)S^{(44)}(k)}{\hbar\omega_3(k)+\epsilon_4(k)}\left[1-\frac{S_F(k)[\tilde{\Gamma}^{(34)}(k)]^2}{S^{(44)}(k)}\right]^2$$

$$\approx -2\frac{\tilde{V}^{(34)}_{\text{p-h}}(k)S^{(44)}(k)}{\hbar\omega_3(k)+\epsilon_4(k)}, \tag{3.7}$$

where $\epsilon_4(k)=t_4(k)/S^{(44)}(k)$ is the Feynman excitation energy, and the last step follows from the dictum to omit all contributions that contain more than one correlated-impurity atom. Alternatively, one may start with Eq. (2.28) that reads, in the single-impurity limit,

$$\chi^{(34)}(k,\omega)=\chi_0^{(33)}(k,\omega)\tilde{V}^{(34)}_{\text{p-h}}(k)\chi^{(44)}(k,\omega), \tag{3.8}$$

use the ''mean-spherical approximation'' (2.26) for the Lindhard function, and calculate $S^{(34)}(k)$ by the frequency integration (2.31). This leads to the same result (3.7). In the strictly low-concentration limit $S_F(k)=1$, $S^{(34)}(k)=\tilde{\Gamma}^{(34)}(k)$, we recover the familiar single-impurity Euler equation[25]

$$S^{(34)}(k)=-2\frac{\tilde{V}^{(34)}_{\text{p-h}}(k)S^{(44)}(k)}{t_3(k)+\epsilon_4(k)}, \tag{3.9}$$

with the particle-hole potential (2.17) and the induced potential,

$$\tilde{w}_{\text{I}}^{(34)}(k)=-\frac{1}{2}\frac{S^{(34)}(k)(S^{(44)}(k)-1)}{S^{(44)}(k)}$$

$$\times[t_3(k)+t_4(k)+\epsilon_4(k)]. \tag{3.10}$$

Equations (3.9), (3.10), and (2.17) form a closed system of equations that can be solved by iteration, given a practical choice for the contributions of the elementary diagrams and triplet correlations to the particle-hole potential, $\Delta V^{(34)}(\mathbf{r}_0,\mathbf{r}_1)$.

Using the PPA equation (2.14) for the background liquid

$$\tilde{V}^{(44)}_{\text{p-h}}(k)=\frac{\hbar^2k^2}{4m_4}\left[\left(\frac{1}{S^{(44)}(k)}\right)^2-1\right] \tag{3.11}$$

we find, in the limit $k\to 0+$

$$S^{(34)}(0+)=-\frac{\tilde{V}^{(34)}_{\text{p-h}}(0+)}{\tilde{V}^{(44)}_{\text{p-h}}(0+)}=-\beta. \tag{3.12}$$

The relation to the volume excess factor in the last equality comes from the identification of the interaction $\tilde{V}^{(34)}_{\text{p-h}}(0+)$ as the effective ^{3}He-^{4}He interaction used by Bardeen, Baym and Pines[24]; see also Chap. 11.5 in Ref. 10.

Finally, we turn to the effective interaction between pairs of impurities. One can again start from a variational wave function that contains two impurities, and then calculate the correlations by minimizing the second-order energy difference

$$\Delta^{(2)}E\equiv E^{II}_{N+2}-2E^{I}_{N+1}+E_N. \tag{3.13}$$

However, this energy difference is only of secondary interest; the physically more relevant quantity is the effective interaction between impurities that can be obtained, in the same manner as outlined above, from the induced interaction (2.18). We proceed again by allowing first for no more than two dynamically correlated impurity particles. Since we are interested in the two-impurity limit of the coordinate-space equation (2.20) that contains already a common factor $\Gamma^{(33)}(r)$, we must not allow for dynamically correlated pairs of impurities in the induced potential. For calculating the induced potential, we must interpret the particle-hole interaction matrix appearing in Eq. (2.18) as being expressed by the PPA equation (2.14). Expanding the (33) component of $\tilde{w}_{\text{I}}^{(33)}(k)$ then leads to

$$\tilde{w}_{\text{I}}^{(33)}(k)=-\frac{[\tilde{\Gamma}^{(34)}(k)]^2}{2S^{(44)}(k)}[2\hbar\omega_3(k)+\epsilon_4(k)]. \tag{3.14}$$

As a further approximation, one may again also ignore statistical correlations by setting $S_F(k)=1$. Then, one arrives at

$$\tilde{w}_{\text{I}}^{(33)}(k)=-\frac{[S^{(34)}(k)]^2}{2S^{(44)}(k)}[2t_3(k)+\epsilon_4(k)], \tag{3.15}$$

which is the induced interaction derived, among others, by Owen.[26]

An alternative derivation, which provides an interpretation of Jastrow–Feenberg theory in terms of Green's functions, is offered by the localizing approximations of parquet-diagram theory.[27–29] The energy-dependent effective interaction between two impurities that is mediated by the exchange of phonons is generally

$$\tilde{V}_{\text{eff}}(k,\omega)=\tilde{V}^{(33)}_{\text{p-h}}(k)+\tilde{V}^{(34)}_{\text{p-h}}(k)\chi^{(44)}(k,\omega)\tilde{V}^{(34)}_{\text{p-h}}(k)$$

$$=\tilde{V}^{(33)}_{\text{p-h}}(k)+\tilde{V}^{(34)}_{\text{p-h}}(k)\frac{2t_4(k)}{(\hbar\omega)^2-[\epsilon_4(k)]^2}\tilde{V}^{(34)}_{\text{p-h}}(k). \tag{3.16}$$

The prescription from parquet-theory to make this energy-dependent interaction local is as follows: Construct the RPA static structure function

$$S^{(33)}_{\rm RPA}(k) = -\int_0^\infty \frac{d(\hbar\omega)}{\pi} {\rm Im}\,[\chi_0^{(33)}(k,\omega) + \chi_0^{(33)}(k,\omega)\tilde{V}_{\rm eff}(k,\omega)\chi_0^{(33)}(k,\omega)]. \quad (3.17)$$

Also, construct the ladder approximation for the same quantity in terms of a different and yet unspecified local effective interaction, say $\tilde{V}_{\rm L}(k)$

$$S^{(33)}_{\rm ladder}(k) = -\int_0^\infty \frac{d(\hbar\omega)}{\pi} {\rm Im}\,[\chi_0^{(33)}(k,\omega) + \chi_0^{(33)}(k,\omega)\tilde{V}_{\rm L}(k)\chi_0^{(33)}(k,\omega)]. \quad (3.18)$$

Now choose an average frequency $\overline{\omega}(k)$ such that these two forms of the static structure function are *identical* for

$$\tilde{V}_{\rm L}(k) = \tilde{V}_{\rm eff}(k,\overline{\omega}(k)). \quad (3.19)$$

The calculation can be carried out in closed form in the collective approximation, leading to

$$V_{\rm L}(k) = V^{(33)}_{\rm p\text{-}h}(k) - 2[\tilde{V}^{(34)}_{\rm p\text{-}h}(k)]^2 S^{(44)}(k) \frac{2\hbar\omega_3(k)+\epsilon_4(k)}{[\hbar\omega_3(k)+\epsilon_4(k)]^2} \quad (3.20)$$

from which we conclude

$$\tilde{w}^{(33)}_{\rm I}(k) = V_{\rm L}(k) - V^{(33)}_{\rm p\text{-}h}(k), \quad (3.21)$$

which is seen to be identical to Eq. (3.14).

The comparison with an energy-dependent interaction not only offers an interpretation of the effective interaction defined by the Jastrow-Feenberg theory in terms of linear-response theory, it also offers a way to relax its approximations. Our analysis shows that Eq. (2.20) is a static approximation for the *energy-dependent* Schrödinger equation

$$\left[-\frac{\hbar^2}{m_3}\nabla^2 + V_{\rm scat}(E_b,r)\right]\phi(\mathbf{r}) = E_b\phi(\mathbf{r}), \quad (3.22)$$

where

$$V_{\rm scat}(E_b,r) \equiv V^{(33)}(r) + w^{(33)}_{\rm I}(E_b,r) + \Delta V^{(33)}(r) \quad (3.23)$$

with

$$\tilde{w}^{(33)}_{\rm I}(E_b,k) = \tilde{V}^{(34)}_{\rm p\text{-}h}(k) \frac{2t_4(k)}{E_b^2 - [\epsilon_4(k)]^2} \tilde{V}^{(34)}_{\rm p\text{-}h}(k) \quad (3.24)$$

is the *energy-dependent* effective potential. The Jastrow-Feenberg wave function approximates this effective interaction with an energy-independent effective interaction such that the static structure function is the same. This is by construction appropriate for the static structure function; it also gives an variational upper bound for the binding energy of the dimer. Since the inclusion of CBF corrections is necessarily perturbative, it is not *a priori* clear whether the energy-dependent effective interaction (3.24) actually improves upon the physical description.

IV. STABILITY ANALYSIS, COLLECTIVE EXCITATIONS, AND DIMER FORMATION

One of the attractive features[30] of modern microscopic many-body theories is that the underlying equations do not have solutions for configurations that are physically unstable. The mixture would, for example, be unstable against the concentration fluctuations if Fermi statistics was turned off. It is therefore not only from the viewpoint of the physical phenomenon, but also from a purely theoretical perspective interesting to study the indications for phase separation and potentially other phase transitions in the mixture and the reflections of such phase separations in the theory. The two-dimensional mixture differs in a number of significant ways from its three-dimensional analog.

When studying the stability of the quantum-liquid mixture, we have to distinguish between *global* and *local* instabilities. A *global* instability means that another phase of the system of a lower energy exists, which the system can reach by a *macroscopic* perturbation of its configuration. In our case, when the chemical potential of a ^{3}He atom in the mixture becomes higher than the chemical potential of the atom in bulk ^{3}He, the mixture will phase separate, but it takes a *finite* external perturbation to initiate the transition. Theoretically, one can detect such an instability only by comparing the ground-state energies of the two different phases.

A *local* instability occurs when the system becomes unstable against *infinitesimal* fluctuations about its equilibrium configuration. Such an instability is indicated by the softening of a collective excitation and should also be reflected in a divergence of the theory. Experimentally, it is very difficult to get close to this second type of an instability since it involves generating an oversaturated mixture. Theoretically, this instability is the more interesting one since it provides a consistency test for the theoretical description.

A. Hydrodynamic stability

The mixture is stable against *infinitesimal* changes of the density and the concentration, if the second derivative matrix of the energy with respect to the concentration and the particle density is positive definite. We write the total energy as a function of ^{4}He and ^{3}He densities

$$E = T_F + E_c[\rho_3,\rho_4], \quad (4.1)$$

where E_c is the correlation energy, and T_F the kinetic energy of the noninteracting fermion component.

We then calculate the *incompressibility tensor*

$$\left(\frac{\sqrt{\rho_\alpha\rho_\beta}}{\Omega}\frac{\partial^2 E}{\partial\rho_\alpha\partial\rho_\beta}\right)_{\alpha\beta} = \begin{pmatrix} \hat{V}^{(33)}(0+) + \dfrac{m_3 c_F^2}{2} & \hat{V}^{(34)}(0+) \\ \hat{V}^{(34)}(0+) & \hat{V}^{(44)}(0+) \end{pmatrix}, \quad (4.2)$$

where $m_3 c_F^2/2=\hbar^2 k_F^2/2m_3$ is the incompressibility of the free Fermi gas, $c_F=\hbar k_F/m_3$ its Fermi velocity, and

$$\hat{V}^{(\alpha\beta)}(0+)\equiv\frac{\sqrt{\rho_\alpha\rho_\beta}}{\Omega}\frac{\partial^2 E_c}{\partial\rho_\alpha\partial\rho_\beta}. \tag{4.3}$$

The eigenvalues of the matrix (4.2) can be related to the ordinary sound velocity c_0 and the second sound velocity c_2. The ''large'' eigenvalue gives the bulk incompressibility $m_4 c_0^2$; it is always positive in the density regime where the liquid is stable against bulk density fluctuations. The ''small'' eigenvalue $m_3 c_2^2$ is related to the second sound velocity that describes concentration fluctuations of the ^{3}He component. We must require $m_3 c_2^2>0$ to guarantee the stability of the mixture against phase separation. For the positivity of the ''small'' eigenvalue, it is sufficient that the determinant of the matrix (4.2) is positive,

$$\pi\frac{\hbar^2\rho_3}{m_3}\frac{\hat{V}^{(44)}(0+)}{[\hat{V}^{(34)}(0+)]^2-\hat{V}^{(33)}(0+)\hat{V}^{(44)}(0+)}>1, \tag{4.4}$$

where we have used that $k_F^2=2\pi\rho_3$.

B. Microscopic stability

A necessary condition for the existence of solutions of the PPA equation (2.14) is that the 2×2 matrix

$$\tilde{\mathbf{V}}_{\text{p-h}}+\frac{1}{2}\mathbf{S_F}^{-1}\mathbf{H_1}\mathbf{S_F}^{-1} \tag{4.5}$$

is positive definite. An instability against density- and concentration fluctuations will first show at small momenta, we therefore calculate the zero-momentum limit,

$$\lim_{k\to 0+}\left[\tilde{\mathbf{V}}_{\text{p-h}}+\frac{1}{2}\mathbf{S_F}^{-1}\mathbf{H_1}\mathbf{S_F}^{-1}\right] = \begin{pmatrix} \tilde{V}^{(33)}_{\text{p-h}}(0+)+\dfrac{\pi^2}{8}\dfrac{m_3 c_F^2}{2} & \tilde{V}^{(34)}_{\text{p-h}}(0+) \\ \tilde{V}^{(34)}_{\text{p-h}}(0+) & \tilde{V}^{(44)}_{\text{p-h}}(0+) \end{pmatrix}. \tag{4.6}$$

Comparison of Eqs. (4.2) and (4.6) suggests the identification $\tilde{V}^{(\alpha\beta)}_{\text{p-h}}(0+)=\hat{V}^{(\alpha\beta)}(0+)$. In fact, the $\hat{V}^{(\alpha\beta)}(0+)$ are the same as the long-wavelength limits of the particle-hole interactions $\tilde{V}^{(\alpha\beta)}_{\text{p-h}}(0+)$ if the Jastrow-Feenberg wave function is optimized for all *n*-body correlations, and if all elementary diagrams are included, in other words in an exact theory. If we identify these interaction terms, the matrices (4.2) and (4.6) differ only in the (33)-channel. The positivity of the matrix (4.2) is clearly the correct stability condition; the discrepancy in the (33)-matrix element of the matrices (4.2) and (4.6) is due to the ''mean-spherical approximation'' discussed above. It is cured by including CBF ring diagrams to all orders in the optimization and requiring that the inverse of the density-density response matrix in Eq. (2.28)

$$[\boldsymbol{\chi}_0(\mathbf{k},\omega)]^{-1}-\tilde{\mathbf{V}}_{\text{p-h}}(\mathbf{k}) \tag{4.7}$$

exists in the long wavelength and zero-frequency limits when the Lindhard function is used for $\chi_0(\mathbf{k},\omega)$.

To highlight the difference between the two- and the three-dimensional system, we assume, for the time being, that a low-concentration mixture exists. We may then further assume that the main concentration dependence of the effective interactions is due to the density factors occurring in the definitions of the $\tilde{V}^{(\alpha\beta)}_{\text{p-h}}(q)$, cf. Eq. (2.16), and in the Fermi velocity c_F. We can therefore write

$$\tilde{V}^{(44)}_{\text{p-h}}(0+)=(1-x)\overline{V}^{(44)}(0+)$$

$$\tilde{V}^{(34)}_{\text{p-h}}(0+)=\sqrt{x(1-x)}\overline{V}^{(34)}(0+)$$

$$\tilde{V}^{(33)}_{\text{p-h}}(0+)=x\overline{V}^{(33)}(0+) \tag{4.8}$$

with $\overline{V}^{(\alpha\beta)}(0+)\equiv\rho\int d^2 r\overline{V}^{(\alpha\beta)}(r)$ and assume that the $\overline{V}^{(\alpha\beta)}(0+)$ do not depend significantly on the concentration *x*. We then get from Eq. (4.6) the stability condition

$$\frac{\pi^3}{8}\frac{\hbar^2\rho}{m_3}\frac{\overline{V}^{(44)}(0+)}{[\overline{V}^{(34)}(0+)]^2-\overline{V}^{(33)}(0+)\overline{V}^{(44)}(0+)}>1. \tag{4.9}$$

Unlike the three-dimensional analog, it is seen that this stability condition is *independent* of the concentration *x*. Hence, the stability condition of the mixture is changed from its zero-concentration limit only by a significant change in the *effective* interactions themselves as a function of concentration and not just by changing the ratio between the Fermi kinetic energy and potential energy as is the case in three dimensions.

C. Dimerization

It was pointed out by Bashkin[31] that pairs of ^{3}He atoms in a dilute ^{3}He-^{4}He mixture will form weakly bound dimers when their motion is restricted to quasi-two dimensions. In particular, the dimerization should occur in a low-density two-dimensional mixture. The effective ^{3}He-^{3}He interaction is a candidate for producing such bound states, to which we shall refer as ''Bashkin-states.'' To prove their existence, we must demonstrate that the sum of the bare interaction, the induced interaction, and the correction originating from elementary diagrams and triplets appearing in Eq. (2.20) is sufficiently attractive. It is relatively easy to see that the elementary diagram contribution falls off at least like r^{-6}, as $r\to\infty$, in other words like the bare interaction. The same proof is also possible, but quite tedious, for the correction from triplet correlations. To calculate the large-distance behavior of the induced interaction term, we study the long-wavelength limit. The considerations go as follows:

First, we realize from Eq. (2.17) that the particle–hole interactions $V^{(44)}_{\text{p-h}}(r)$ and $V^{(34)}_{\text{p-h}}(r)$ are short-ranged functions that fall off at least as r^{-6} as $r\to\infty$, hence their Fourier transforms go as

$$\tilde{V}^{(\alpha\beta)}(k)=a_{\alpha\beta}+b_{\alpha\beta}k^2+O(k^4), \tag{4.10}$$

where we can identify $a_{44}=m_4c_0^2$ and $a_{34}=\beta m_4 c_0^2$, cf. Eq. (3.12), where c_0 is the speed of sound. Inserting these expansions into Eq. (3.15) yields a small k expansion

$$\tilde{w}_{\rm I}^{(33)}(k)=-\beta^2 m_4 c_0^2+\text{const}\times k^2-\frac{\beta^2\hbar^3 m_4}{4m_3^3 c_0}k^3+\mathcal{O}(k^4), \tag{4.11}$$

from which we conclude that

$$\tilde{w}_{\rm I}^{(33)}(r)\sim-\frac{9\beta^2\hbar^3 m_4}{8\pi\rho m_3^3 c_0}r^{-5}+\mathcal{O}(r^{-6}) \quad \text{as} \quad r\to\infty, \tag{4.12}$$

in other words, the *phonon-induced* interaction dominates the effective interaction for $r\to\infty$ and is attractive.

Things change, as they should, if Fermi statistics is included. First, the ''Schrödinger-equation'' (2.20) for the coordinate-space correlations is no longer rigorously valid as pointed out above. But even if one ignores this, it is no longer possible to prove that $w_{\rm I}^{(33)}(r)$ is attractive and dominates for large distances. Using Eqs. (3.14) and (3.7) instead of Eqs. (3.15) and (3.9), one finds that the small k expansion of $\tilde{w}_{\rm I}^{(33)}(k)$ has only even powers up to k^4. In other words, the phonon-induced interaction gets effectively screened by Fermi statistics. In practice one has, of course, a smooth transition between the rigorously dilute limit and the case of a weakly interacting Fermi gas, the crossover being at ^{3}He concentrations where the size of the dimer becomes comparable to the inverse of the Fermi wave vector.

One might therefore expect that dimerization is a rather exotic effect that happens only at very small concentrations, and in the microkelvin regime. Our stability analysis of the previous section comes to bear at this juncture: If the ^{3}He component forms a two-body bound state, then it can also form a many-body bound state that would be detected as a spinodal decomposition of the mixture. Above, we have shown that it needs macroscopic changes of the effective interactions to change the inequality (4.9). Therefore, while superficially a subtle effect, we expect a rather robust phenomenon.

In conclusion of this section, we point out that a very similar dimerization effect has been discussed in astrophysical ^{4}He plasmas, where an instability of the coordinate-space Euler equation was interpreted as a phase transition to stable ^{8}Be matter.[32,33]

V. GROUND-STATE RESULTS

A. ^{4}He in two dimensions

To demonstrate the validity of the predictions of the semianalytic microscopic methods of the kind presented here we can utilize simulation data for the two-dimensional liquids ^{4}He and ^{3}He. The best results available today are the diffusion Monte Carlo (DMC) calculations for ^{4}He of Giorgini *et al.*[34] and some very recent results[35] on two-dimensional ^{3}He.

Figure 1 shows the two-dimensional equation of state calculated from the Aziz-II potential of Ref. 9 and compares with the Monte Carlo evaluation of Giorgini *et al.*[34] The agreement is not quite as perfect as the one obtained for the older Aziz potential,[8] but it is still quite satisfactory. The same holds for the derived quantities, pressure per density p/ρ and the chemical potential μ_4 which are also shown in Fig. 1. Note that the HNC-EL results for the pressure and the chemical potential were derived by diagrammatic differentiation of the working formulas of the theory, and not by numerically differentiating the equation of state.

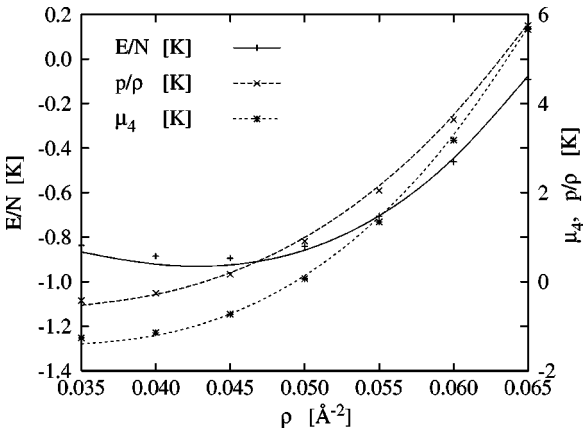

FIG. 1. The figure shows the HNC-EL results for the energy per particle E/N, (solid line, left scale), the pressure per density p/ρ (long-dashed line, right scale) and the chemical potential μ_4 (short-dashed line, right scale). Also shown are DMC data from Ref. 34 for the energy (+ symbols), the pressure per density (crosses) and the chemical potential (stars). All energies are given in degrees Kelvin.

Similarly good agreement between our HNC-EL results and DMC data is obtained for the pair-distribution function $g^{(44)}(r)$ and the static structure function $S^{(44)}(k)$; Fig. 2 shows, as an example, a comparison of $g^{(44)}(r)$ at three different densities. The agreement is quite satisfactory especially in the regime up to the nearest-neighbor peak. At larger distances, our results appear to be shifted slightly inwards. Figure 3 shows a comparison of the static structure functions; consistent with the slight shift of the oscillations

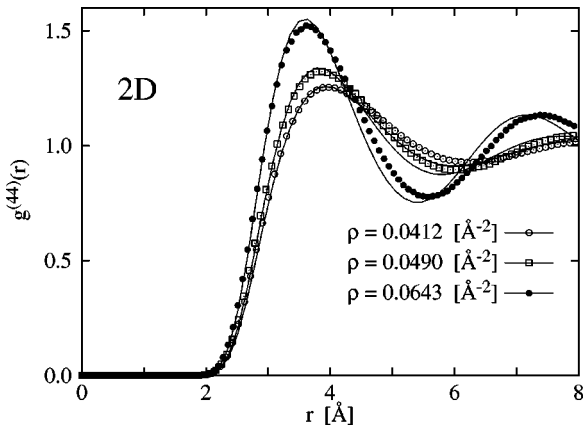

FIG. 2. The HNC-EL results for the pair-distribution function $g^{(44)}(r)$ (solid lines) are compared with DMC data (markers) at the three densities $\rho=0.0412$ Å^{-2}, $\rho=0.0490$ Å^{-2}, and $\rho=0.0643$ Å^{-2}.

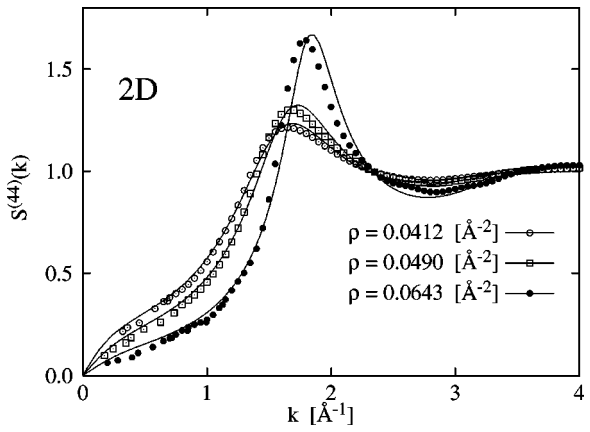

FIG. 3. The HNC-EL results for the static structure function $S^{(44)}(k)$ (solid lines) are compared with DMC data (markers) at the three densities $\rho=0.0412$ Å^{-2}, $\rho=0.0490$ Å^{-2}, and $\rho=0.0643$ Å^{-2}.

of $g^{(44)}(r)$ we find a slight outward shift of the peak of $S^{(44)}(k)$ in the HNC-EL calculation.

B. Single-impurity calculation

The calculation of the chemical potential of a single ^{3}He impurity proceeds along the same lines as in the three-dimensional case.[25] Since the physical effects to be described here are quite delicate, and since no simulation data are available at this time for a direct comparison, we need to be particularly careful with the verification of our results.

The accuracy of our results can be estimated by using the ''average-correlation approximation (ACA)'' for calculating a rigorous upper bound for the impurity chemical potential as follows: Let $\Psi_{N+1}(\mathbf{r}_0,\ldots,\mathbf{r}_N)$ be the ground-state wave function of $N+1$ ^{4}He atoms, and $\Psi^I_{N+1}(\mathbf{r}_0,\ldots,\mathbf{r}_N)$ the ground state of N ^{4}He and one ^{3}He impurity, approximated, for example, by the variational function (3.1). Then, the impurity chemical potential μ_3^I can be estimated as[36,37]

$$\begin{aligned}\mu_3^I &\equiv \langle\Psi^I_{N+1}|H^I_{N+1}|\Psi^I_{N+1}\rangle-\langle\Psi_N|H_N|\Psi_N\rangle\\ &\leqslant \langle\Psi_{N+1}|H^I_{N+1}|\Psi_{N+1}\rangle-\langle\Psi_N|H_N|\Psi_N\rangle\\ &= \left(\frac{m_4}{m_3}-1\right)\langle T_4\rangle+\mu_4\equiv\mu_3^{ACA},\end{aligned} \tag{5.1}$$

where $\langle T_4\rangle$ is the kinetic energy per particle of the ^{4}He component, and μ_4 is the ^{4}He chemical potential. Both quantities can be obtained from simulations[34] without recourse to semianalytic theories, but, of course, also within our theoretical framework. That way, we can reassure the accuracy of our calculations in two ways. First, by asserting that our ACA estimate for the ^{3}He chemical potential agrees sufficiently well with what one would obtain from Ref. 34. Second, the relevant quantity is only the *increase* of the ^{3}He binding due to relaxing the ACA, and the energy differences gained by relaxing the ACA should be more accurate than the absolute energies. Since we have already verified above that the chemical potential of the ^{4}He component agrees well with those of Ref. 34, we only need to show that the kinetic energies agree equally well. Figure 4 shows the comparison that is evidently accurate for all practical purposes.

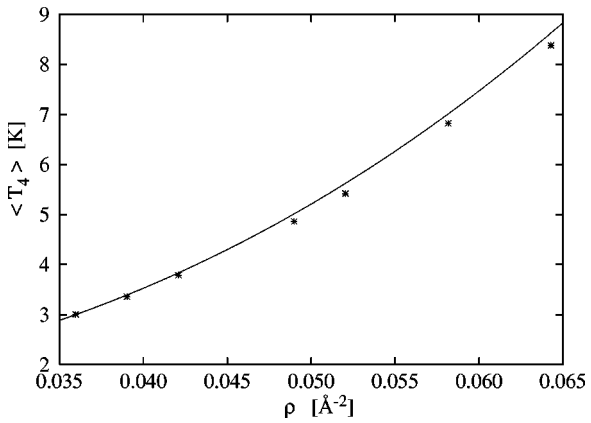

FIG. 4. The kinetic energy of two-dimensional ^{4}He resulting from our HNC-EL calculation (solid line) is compared with the DMC results of Ref. 34 (stars).

In Figure 5 we compare the full calculation of the ^{3}He chemical potential with the ACA result. The gain in energy due to relaxing the ACA is about 0.2–0.3 K in the whole density range. As expected, Monte Carlo results for the ACA are slightly below our approximate result and thus we can conclude that our full calculation gives a reliable upper bound for μ_3^I.

After these rigorous estimates of the impurity chemical potential we are ready to compare μ_3^I with the chemical potential of the pure ^{3}He gas, $\mu_3^{\rm pure}$. Recent Monte Carlo simulations are available for the energy per particle as a function of density[35] from which we can calculate $\mu_3^{\rm pure}(P)$. In Fig. 6 we show the *difference* between these chemical potentials,

$$\Delta\mu(P)=\mu_3^I(P)-\mu_3^{\rm pure}(P), \tag{5.2}$$

as a function of pressure for different approximations. A positive $\Delta\mu$ indicates phase separation, whereas a negative

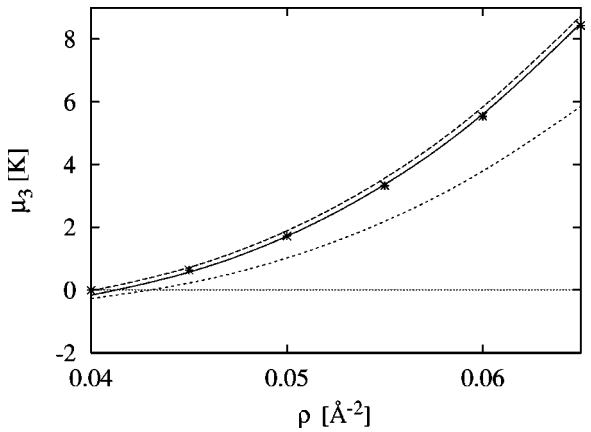

FIG. 5. The ^{3}He impurity chemical potentials as a function of density. The result of the full calculation (solid line) is compared with the average-correlation approximation (long-dashed line). The stars give the average-correlation approximation of the Monte Carlo simulations Ref. 34. Also plotted in the figure is the pressure/density (short dashed line).

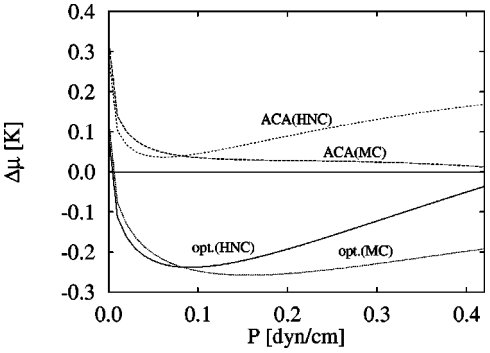

FIG. 6. The difference $\Delta\mu$ between the ^{3}He impurity chemical potentials and the pure ^{3}He chemical potential is shown as a function of pressure. The solid line shows the result of the fully optimized (F)HNC-EL calculation. The short-dashed line is our ACA estimate (5.1), the long-dashed line is the ACA estimate (5.1) from Monte Carlo simulations of pure ^{4}He, and the dotted line is the estimate for $\Delta\mu$ obtained by supplementing the ACA from Monte Carlo results by our enhancement of the binding due to relaxing the ACA as defined in Eq. (5.3).

$\Delta\mu$ indicates mixing. The ACA using Monte Carlo yields a rigorous upper limit for the impurity chemical potential that is less than 0.1 K above $\mu_3^{\rm pure}(P)$ for pressure $P>0.002$ dyn/cm. Our result for μ_4 gives a slightly higher upper limit as also shown in Fig. 6.

The situation changes when the impurity-background correlations are optimized. As pointed out earlier, the chemical potential is lowered by 0.2–0.3 K by relaxing the ACA. At zero pressure, the ^{3}He impurity chemical potential is still positive, $\mu_3^I \approx +0.13K$, whereas the chemical potential of the pure ^{3}He gas approaches zero proportional to $\sqrt{P}$. This means that no stable mixture can exist at zero pressure. But, with increasing pressure, the ^{3}He chemical potential in the pure phase increases faster than that of the impurity, and the mixture becomes stable for pressures $P>0.002$ dyn/cm. The maximum difference in the chemical potentials is ≈ -0.25 K at $P=0.1$ dyn/cm; we can therefore conclude that the mixture is stable at pressures $P>0.002$ dyn/cm and phase separates at very low pressures.

The most realistic estimate is obtained by supplementing the ACA from Monte Carlo data with our correction of the chemical potential due to relaxing the ACA, i.e., we define

$$\Delta\mu_{\rm opt}(MC) \equiv \Delta\mu_{\rm ACA}(MC) + [\Delta\mu_{\rm opt}(HNC) - \Delta\mu_{\rm ACA}(HNC)]. \quad (5.3)$$

This leads to the dotted line in Fig. 6, which favors mixing most strongly over a wide regime of pressures.

Differences between the radial distribution functions $g^{(44)}(r)$ and $g^{(34)}(r)$ after the full optimization are quite visible as shown in Fig. 7. The height of the peak in $g^{(34)}(r)$ is clearly lower and slightly shifted towards larger r, which is consistent with the fact that a ^{3}He impurity makes a bigger correlation hole than a ^{4}He atom due to the stronger zero-point motion. The effect is seen more clearly in the static structure functions of Fig. 8. The value $S^{(34)}(0+) = -\beta$ gives the volume excess factor for the impurity. At these two representative densities $\rho=0.0412$ Å^{-2} and $\rho=0.0643$ Å^{-2} we find $\beta=1.63$ and $\beta=1.25$, respectively. The peaks of the ^{3}He structure functions are also lower than for ^{4}He.

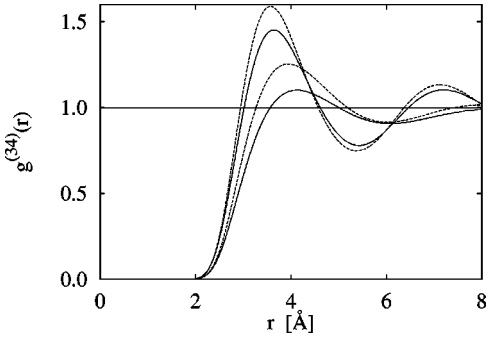

FIG. 7. The HNC-EL results for the ^{3}He impurity pair-distribution functions $g^{(34)}(r)$ (solid lines) for two densities $\rho=0.0412$ Å^{-2} and $\rho=0.0643$ Å^{-2}. The higher peak corresponds to the higher density. For comparison we have plotted also the ^{4}He pair distribution functions $g^{(44)}(r)$ at the same densities (dashed lines).

C. Two impurities

We have discussed in Sec. (IV C) the mechanism of the dimer formation from the point of view of the long-range attraction induced by the phonon exchange. The phonon exchange is sufficient to bind ^{3}He dimers. However, the much shorter-ranged contribution $\Delta V^{(33)}(r)$ causes a quantitatively significant increase of the dimer binding energy, which is strongly density dependent as shown in Fig. 9. When only the bare interaction and induced potential $w_{\rm I}^{(33)}(r)$ from HNC approximation are included, the binding energy is about two orders of magnitude smaller than from the full calculation. Yet, one should realize that the saturation density in the HNC approximation is at much lower density, 0.032 Å^{-2}, and at that density the dimer binding is 232 μK.

In the full calculation zero pressure corresponds to the density $\rho=0.043$ Å^{-2} in agreement with simulations. The dimer binding at that density is ≈ 26 μK. The binding en-

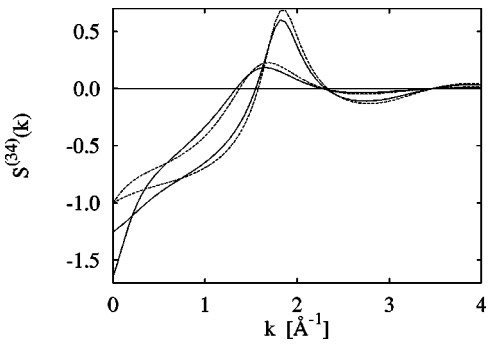

FIG. 8. The HNC-EL results for the ^{3}He impurity-structure functions $S^{(34)}(k)$ (solid lines) for two densities $\rho=0.0412$ Å^{-2} and $\rho=0.0643$ Å^{-2}. The higher peak corresponds to the higher density. For comparison we have plotted also $S^{(44)}(k)-1$ at the same densities (dashed lines).

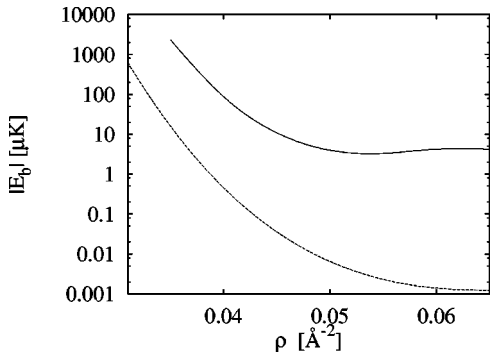

FIG. 9. The binding energy of a dimer of ^{3}He atoms within two-dimensional ^{4}He in logarithmic scale as a function of density. The solid line is the result of the full calculation, the dashed line shows the result from the HNC approximation, omitting the corrections $\Delta V^{(33)}(r)$ from the elementary diagrams and triplet correlations.

ergy decreases with increasing density; one reason for this is that the attraction of the asymptotic tail of the phonon-induced interaction decreases since the volume-excess factor decreases and the speed of sound increases with increasing density. Near the solidification density oscillations of the effective interaction build up; they extend further and further out into the tail and also reduce the binding. Since the dimer is very weakly bound, its wave function decays very slowly. Figure 10 shows the wave function for three different densities. They show a maximum at $\approx$4 Å that coincides with the first maximum of the radial distribution function of the pure ^{4}He. From the wave function we can calculate the root-mean-square (rms) radius of the dimer $\sqrt{\langle r^2\rangle}$. The main contribution to the integral comes from the tail of the wave function $\phi(\mathbf{r}) \sim K_0(\sqrt{2m_3|E_b|/\hbar^2}r)$ and that gives a simple approximation

$$\sqrt{<r^2>} \approx \sqrt{\frac{\hbar^2}{3m_3|E_b|}}, \tag{5.4}$$

which is accurate within 3% for the whole density range. The value of the rms radius increases from 70 Å at the density 0.035 Å^{-2} to 1000 Å at 0.065 Å^{-2}.

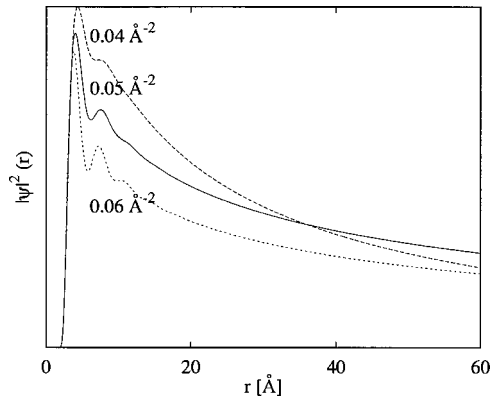

FIG. 10. The square of the ^{3}He wave function for three different ^{4}He densities as marked in the figure.

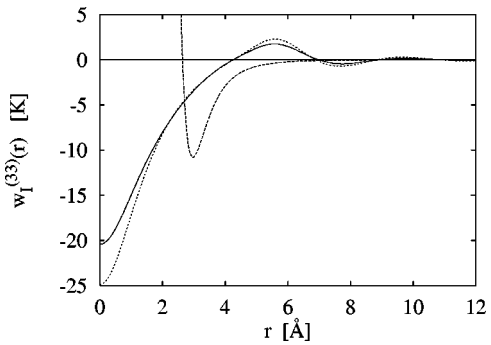

FIG. 11. Comparison of the energy-dependent induced potential from Eq. (3.24) (short dashed line) with the (F)HNC result of Eq. (3.15) (solid line). Also shown is the bare two-particle interaction (dashed line).

An alternative derivation of the effective interaction based on Green's functions led to the energy-dependent interaction of Eq. (3.16). Since the dimer binding is a very low energy phenomenon one is tempted to approximate the binding energy in the energy-dependent interaction (3.24) by zero. This clearly gives an induced potential that is more attractive in k space. However, this increase in the attraction is, in configuration space, hidden behind the strong repulsion of the bare interaction at small r as shown in Fig. 11. Thus we find no bound state in that zero-energy limit. Since the variational theory produces an upper bound for the binding energy, we conclude that relaxing the approximations implicit to that theory—specifically the ''localization'' of effective interactions by introducing an average energy—do not necessarily improve the physical description of the system.

Fermi statistics is expected to screen the interaction between pairs of impurities at finite concentrations. We can estimate this effect by using the induced interaction from Eq. (3.14) together with Eq. (3.7) and get the low-concentration dependence of the dimer binding energy. This estimate is valid only up to 2–3 % concentrations, because we have assumed that the particle-hole interactions $\tilde{V}^{(44)}_{\text{p-h}}(k)$ and $\tilde{V}^{(34)}_{\text{p-h}}(k)$ as well as the higher-order correlation effects, $\Delta V^{(44)}(k)$ and $\Delta V^{(34)}(k)$ remain independent of concentration. The results are shown in Fig. 12. At one percent concentration the binding energy has dropped roughly to half. In

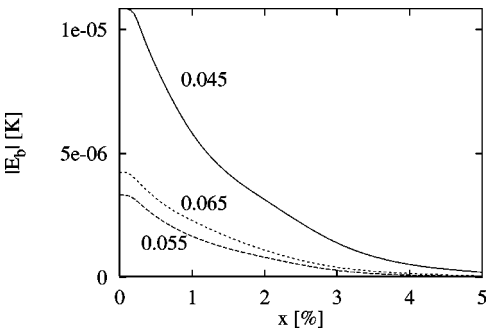

FIG. 12. The concentration dependence of the binding energy of a ^{3}He dimer within two-dimensional ^{4}He for three different densities, 0.045, 0.055, and 0.065 Å^{-2}, marked in the figure. These results were obtained assuming a dilute Fermi gas of ^{3}He atoms.

the full finite concentration mixture calculation discussed in the next section we find that the homogeneous *atomic* mixture becomes stable at concentrations above 2–3 % and the dimer binding vanishes.

We have shown that the binding energy of the dimer depends very strongly on the density and the best possibility of finding a dimer state is at very low densities and concentrations. The estimate for the concentration dependence in the low-concentration limit complements the discussion of the next section in the sense that it demonstrates, again, the *robustness* of the dimerization effect showing that it does not disappear at infinitesimal concentrations.

D. Finite-concentration mixtures

The examination of the single- and two-impurity limits and the comparison of the energetics and effective interactions has lead to two conclusions: First, at slightly positive pressures, the chemical potential of a single ^{3}He impurity in the mixture is less than that in the two-dimensional ^{3}He at the same pressure, which means that the mixture will not phase separate into disjoint regions of ^{4}He and ^{3}He. Second, the effective interaction between pairs of ^{3}He impurities is sufficiently attractive such that these impurities form dimers. Both of these conclusions were independent of the theoretical tools and based on either simulation data or rigorous upper bounds. Among others, our analysis demonstrates that an *atomic mixture* of ^{3}He and ^{4}He is, in two dimensions and at sufficiently low concentrations, unstable against dimerization, but stable against phase separation.

As the concentration is increased, one expects that the dimers dissolve and an atomic mixture is formed. A full microscopic theory is required for calculating the properties of such a mixture. The accuracy of our calculation of the ^{4}He component has been demonstrated above, there is therefore only need to estimate the concentrations for which we expect that the calculations of the ^{3}He component are reliable. We have used the version of the (F)HNC-EL theory explained in detail in Ref. 6. The method implies, for the fermion channels, a simplified version of the FHNC-EL equation that is not sufficiently accurate for a quantitative description of pure ^{3}He in three dimensions. We can indirectly assess the expected accuracy of our calculations as follows: In the three-dimensional mixture, we have demonstrated the accuracy of our results for the energy up to 20 atm pressure, corresponding to a density of approximately 0.026 Å^{-3}, and up to 10% concentration. The average distance between ^{3}He atoms is, at this density, about 4.5 Å . This translates to a ^{3}He density of 0.016 Å^{-2} in two dimensions, which is about 25% of the solidification density of 0.065 Å^{-2}. A conservative estimate would then lead us to expect that our calculations are similarly accurate as those of Ref. 6 up to about 25% concentration.

Results for the equation of state $E(\rho,x)/N$, the chemical potential of the ^{3}He-component $\mu_3(\rho,x)$, and the speed of second sound mc_2^2 are shown in Figs. 13, 14, and 15. The most interesting result is the concentration dependence of the second sound speed. As pointed out above, it is unavoidable that the system exhibits a *local* instability at low concentrations, coming from above. Figure 15 shows, for three different densities, the long-wavelength limit of mc_2^2 as a function of concentration for both the (F)HNC-EL calculation and the CBF corrected calculations. It is very difficult to get close to the actual phase transition because this instability is driven by the appearance of the ^{3}He-^{3}He dimer. This can be seen

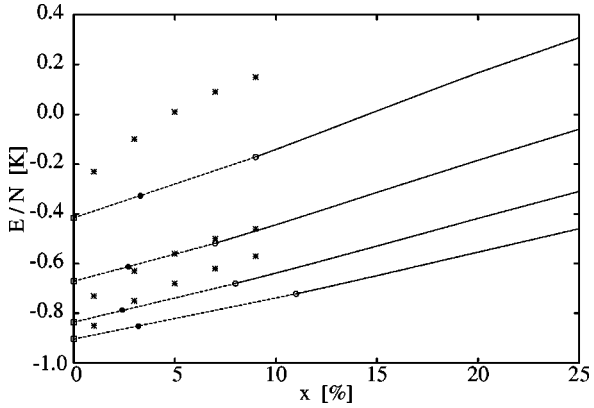

FIG. 13. The energy per particle of the two-dimensional mixture is shown, for the densities ρ=0.045, 0.050, 0.055, and 0.060 Å^{-2}, as a function of concentration x. The highest line corresponds to the highest density, the boxes at the left margin are the results for pure two-dimensional ^{4}He. The unstable area between the zero-concentration limit and the estimated spinodal point for phase separation is dashed, the estimated spinodal concentrations are indicated by heavy dots, whereas the end point of our numerical calculations is indicated by an open circle. Also shown are the (F)HNC results of Ref. 38 for the densities ρ=0.045, 0.50, and 0.60 Å^{-2}.

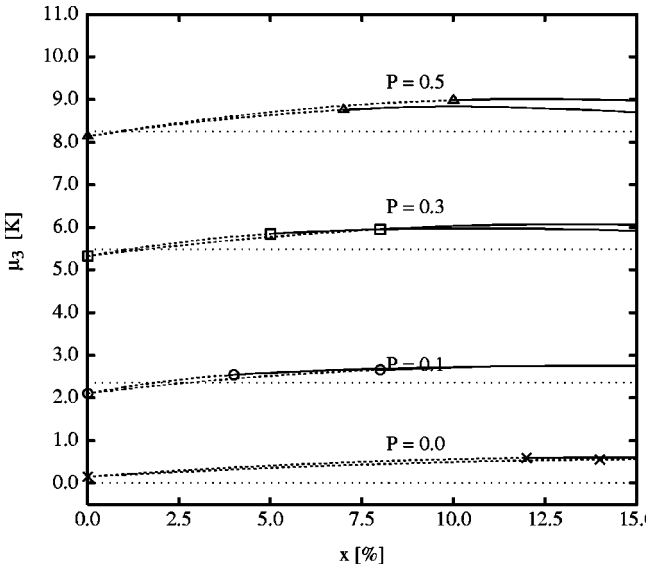

FIG. 14. The chemical potential of the ^{3}He component of the two-dimensional mixture is shown, as a function of concentration x, for the pressures 0.0, 0.1, 0.3, and 0.5 dyn/cm in (F)HNC-EL calculation and in the CBF-corrected calculation. The results have been smoothly interpolated through the unstable region to match the $x=0$ value. The interpolated region is drawn as dashed lines and ended by markers. The CBF-corrected chemical potentials are slightly higher. Four dotted horizontal lines show the chemical potentials of the pure ^{3}He gas at the indicated pressures from Ref. 35.

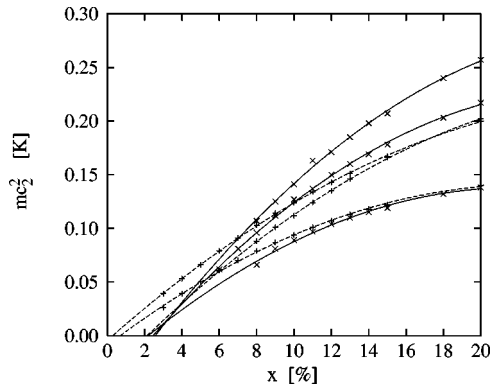

FIG. 15. The speed of second sound of the two-dimensional mixture is shown, for the densities ρ=0.045, 0.055, and 0.065 Å^{-2}, as a function of concentration x for both the (F)HNC-EL calculation (+ symbols) and the CBF-corrected calculation (crosses). Also shown are the fits to these data that determine the estimates for the lowest concentration that is stable against concentration fluctuations (dashed and solid lines, respectively).

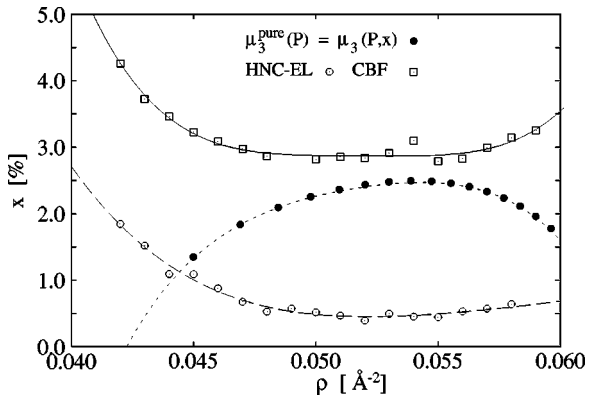

FIG. 16. The figure shows the extrapolated critical concentration where the atomic mixture becomes unstable against infinitesimal concentration fluctuations. The squares and circles show the actually extrapolated values from the CBF and FHNC-EL calculation, respectively; the long dashed and the solid line give a smooth interpolation of these results. The short-dashed line marked with filled dots gives the upper bound of the concentration below which the mixture is globally stable.

from Eq. (2.19) as follows: In the small concentration limit, the factor $S_F^{-1}(k)$ in Eq. (2.19) can be ignored, and the equation turns into an ordinary Schödinger equation with an effective potential. The boundary condition in a many-body system is $\sqrt{1+\Gamma_{dd}(r)}\to 1$ as $r\to\infty$. On the other hand, the solution of Eq. (2.20) diverges logarithmically unless the integral

$$\int_0^\infty dr\, r V_{scat}(r)\sqrt{1+\Gamma_{dd}(r)}, \tag{5.5}$$

of the effective interaction is zero. However, the above integral cannot be zero because the interaction has demonstrably a bound state at $x\to 0$. This means that the solutions of the Euler equations start to build up a much stronger long-ranged behavior than in three dimensions. This is the reason why it is very difficult to get close to the spinodal density since this would require huge simulation volumes. To remain practical, we have worked here with a cut-off radius of 100 Å . One must therefore rely on an extrapolation in order to determine the critical concentration, which implies some numerical uncertainty.

For the purpose of this extrapolation, we have fitted the mc_2^2 in the regime where the calculations could be done with a reasonable effort to a polynomial of the order

$$mc_2^2(x)=a(x-x_0)+b(x-x_0)^2. \tag{5.6}$$

Our estimates for the critical concentration, as a function of density, are shown in Fig. 16. With all the caution that should be exercised when relying on extrapolations, we assert that the FHNC-EL approximation predicts a critical concentration of 1–2 %, below which the atomic mixture is unstable. A better CBF calculation predicts a somewhat steeper functional form of $mc_2^2(x)$ and, hence, a higher critical concentration. Because of this steeper behavior, it is numerically even harder to get close to the spinodal point. The CBF results have been derived from an extrapolation that reaches much farther and has, hence, larger uncertainties. This is also clearly seen from Fig. 16 from the larger scatter of the results.

The horizontal lines in Fig. 14 show the chemical potential of pure ^{3}He gas at the indicated pressures. At finite pressures and low concentrations the mixture is *globally* stable against phase separation. When the concentration increases, the ^{3}He chemical potential in the mixture exceeds the one in the pure ^{3}He gas. These critical concentrations vary between zero and 2.5% depending on the pressure. Figure 16 shows a more complete set of results that determine the upper bound for the globally stable mixture at zero temperature.

Compared with the stability of the mixture, its energetics is of lesser interest because, in reality, the energetics of an atomic monolayer is dominated by its external holding potential. Figure 13 shows the energy per particle as a function of density and concentration. We only show the variational results; the CBF corrections are, on the scale of the figure, too small to be distinguishable. This is not unexpected because the approximations underlying the Jastrow-Feenberg wave function (specifically, the ''mean-spherical'' or ''collective'' approximation discussed in Sec. II B) are particularly good when it comes to calculating integrated quantities like the energy, whereas they are particularly poor when it comes to calculating effects for which the existence of a Fermi surface is important.

Figure 13 also shows the energetics of the two-dimensional ^{4}He liquid to demonstrate that both calculations are consistent; the unstable regime between the estimated spinodal concentration and the zero-concentration limit has been bridged by a smoothly interpolating dashed line. We also show the results of a recent similar calculation by Um *et al.*[38] This calculation uses parametrized pair and triplet correlation functions that are the same for all combinations of ^{3}He and ^{4}He atoms ''ACA,'' and a ''scaling'' procedure for the elementary diagrams similar to that introduced in Ref. 6 to reproduce the equation of state of two-dimensional ^{4}He.

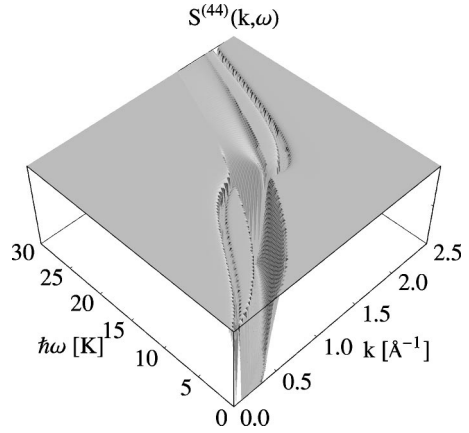

FIG. 17. The dynamic structure function $S^{(44)}(k,\omega)$ is shown for a density of 0.050 Å^{-2} and 10% concentration of ^{3}He atoms. Note that the $S^{(44)}(k,\omega)$ axis points downward, the units in that direction are arbitrary.

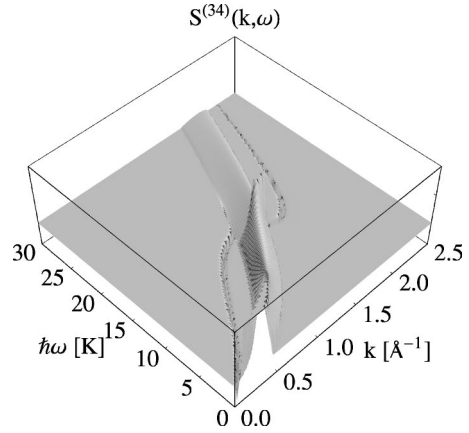

FIG. 18. Same as Fig. 17 for $S^{(34)}(k,\omega)$.

It is not the purpose of this work to discuss the *pros* and *cons* of various approximation schemes, but it seems to us that the ACA is the main reason that the equation of state comes out stiffer in that work. Recall also that we needed to abandon the ACA in order to demonstrate that the ^{3}He impurity in ^{4}He has, at finite pressure, a lower chemical potential than in pure ^{3}He. The much richer physics coming out of the optimized (F)HNC-EL gives striking testimony for the power of the method, considering, in particular, that the technical effort going into the calculation is comparable.

VI. DYNAMICS OF SINGLE IMPURITIES AND THE MIXTURE

A part of the theoretical description of the mixture is the calculation of dynamic features; and we include a discussion of these features for completeness. We note, however, that the discussion that follows applies to *isolated* atoms and *homogeneous* atomic mixtures; an experimental verification of these features depends therefore on whether one succeeds in dissolving the ^{3}He dimers or by stabilizing the metastable finite-concentration regime. Scenarios for how such a systems could be formed will be discussed at the end of this paper.

A. Dynamic structure functions

It is seen from Eq. (2.28) that the calculation of an RPA for the dynamic structure function $S(k,\omega)$ is an integral part of the theory. The RPA is, of course, a fairly simple approximation and reproduces the dynamics of the mixture only qualitatively, typically within a factor of 2 in the energy scale. For a description that is both qualitatively more accurate and physically more complete, it is necessary to allow for *time-dependent* pair correlations[39] $\delta u^{(\alpha\beta)}(\mathbf{r}_i,\mathbf{r}_j;t)$.

The dynamic structure function $\mathbf{S}(k,\omega)$ defined in Eq. (2.30) is calculated along with the calculation of the CBF corrections to the energy. Figures 17, 18 and 19 show three-dimensional plots of the components $S^{(\alpha\beta)}(k,\omega)$, the results are qualitatively similar to those obtained in three dimensions. The sound mode is discrete; to show its strength in the three channels, we have artificially broadened the δ function describing the dispersion relation by a Gaussian of 2 K width and the strength of the δ function.

In particular, we see in the (44) channel that the contribution of the particle-hole continuum is significant. We believe that the relative strength between the discrete sound mode and the particle-hole continuum is reasonably well represented by the RPA, but a definite resolution of the problem can, of course, be obtained by extending the CBF theory of collective excitations[40] to the case of fermions and mixtures.

B. Hydrodynamic effective mass

Time-dependent pair correlations are also necessary to describe the motion of impurities in the liquid. The theory has been worked out for this simple system in much more detail than for the dynamic structure function $S(k,\omega)$ of the finite-concentration boson-fermion mixture since the *dominant* physical effect is the hydrodynamic backflow. Fermi-liquid effects are less important and can, hence, be dealt with in a simpler approximation.

A natural generalization of the wave function (3.1) for a moving impurity atom is to allow for *time-dependent* correlations. The *kinematic* and *dynamic* correlations are separated by writing the wave function in the form

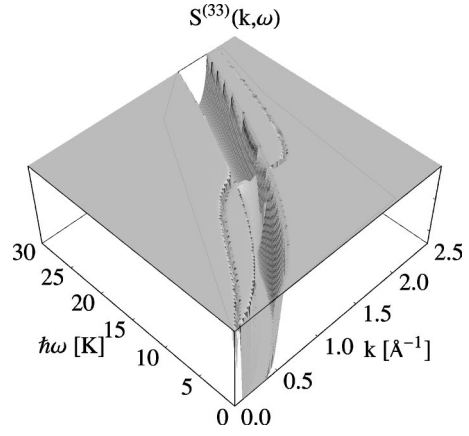

FIG. 19. Same as Fig. 17 for $S^{(33)}(k,\omega)$.

$$\Phi(t)=\exp\{-iE^I_{N+1}t/\hbar\}\Psi^I_{N+1}(\mathbf{r}_0,\mathbf{r}_1,\ldots\mathbf{r}_N;t)/\sqrt{\langle\Psi^I_{N+1}(t)|\Psi^I_{N+1}(t)\rangle}, \tag{6.1}$$

where $\Psi^I_{N+1}(\mathbf{r}_0,\mathbf{r}_1,\ldots\mathbf{r}_N;t)$ contains the time-dependent correlations,

$$\Psi^I_{N+1}(\mathbf{r}_0,\mathbf{r}_1,\ldots\mathbf{r}_N;t) = \exp\frac{1}{2}\left[\delta u^{(3)}(\mathbf{r}_0;t)+\sum_{i=1}^{N}\delta u^{(34)}(\mathbf{r}_0,\mathbf{r}_i;t)\right] \times\Psi^I_{N+1}(\mathbf{r}_0,\mathbf{r}_1,\ldots,\mathbf{r}_N). \tag{6.2}$$

The time-dependent components of the wave function are determined by an action principle, searching for a stationary value of the action integral

$$\mathcal{L}=\int dt\langle\Phi(t)|H^I_{N+1}+U_{\rm ext}(\mathbf{r}_0;t)-i\hbar\frac{\partial}{\partial t}|\Phi(t)\rangle. \tag{6.3}$$

The details of the theory as well as the relationship of the resulting equations to Green's functions theories have been worked out in Ref. 41. The dispersion relation of the particle is determined by the implicit equation

$$\hbar\omega(k)=\frac{\hbar^2k^2}{2m_3}+\Sigma^{(3)}(k,\omega(k)) \tag{6.4}$$

with the self-energy

$$\Sigma^{(3)}(k,\omega)=\frac{\hbar^2}{2m_3}\int\frac{d^2p}{(2\pi)^2\rho_4}\frac{\mathbf{k}\cdot\mathbf{p}S^{(34)}(p)\beta^{(34)}_{\mathbf{k},\omega}(\mathbf{p})}{[\hbar\omega-t_3(\mathbf{k}+\mathbf{p})-\epsilon_4(p)]}. \tag{6.5}$$

The function $\beta^{(34)}_{\mathbf{k},\omega}(\mathbf{p})$ defined in Ref. 41 is related to the ratio of the Fourier transform of the fluctuating two-particle correlation function and the single-particle density, $\delta\rho_3(k,\omega)$

$$\frac{\beta^{(34)}_{\mathbf{k},\omega}(\mathbf{p})\,\delta\rho_3(k,\omega)}{\hbar\omega-t_3(\mathbf{k}+\mathbf{p})-\epsilon_4(p)} =\rho_3\rho_4\int d^2r_0d^2r_1dt\exp[-i(\mathbf{k}\cdot\mathbf{r}_0+\mathbf{p}\cdot(\mathbf{r}_0-\mathbf{r}_1)-\omega t)] \times\delta u^{(34)}(\mathbf{r}_0,\mathbf{r}_1;t). \tag{6.6}$$

In the limit $k\to0$, it can be calculated from the integral equation

$$\beta^{(34)}_{\mathbf{k},\omega_0}(\mathbf{p})=\hbar\omega_0\frac{\mathbf{k}\cdot\mathbf{p}}{k^2}\frac{S^{(34)}(p)}{S^{(44)}(p)} -\int\frac{d^2q}{(2\pi)^2\rho_4}\frac{\mathbf{p}\cdot\mathbf{q}}{p^2}\frac{\beta^{(34)}_{\mathbf{k},\omega_0}(\mathbf{q})K(\mathbf{p},\mathbf{q})}{t_3(\mathbf{q})+\epsilon_4(q)} \tag{6.7}$$

with the kernel

$$K(\mathbf{p},\mathbf{q})=t_3(p)S^{(44)}(q)\{[S^{(34)}(|\mathbf{p}-\mathbf{q}|)+1]\tilde{u}^{(344)} \times(\mathbf{p}-\mathbf{q},-\mathbf{p},\mathbf{q})+S^{(34)}(|\mathbf{p}-\mathbf{q}|)\} +\epsilon_4(p)S^{(34)}(|\mathbf{p}-\mathbf{q}|). \tag{6.8}$$

The low-momentum limit of the dispersion relation defines the *hydrodynamic* effective mass

$$\hbar\omega(k\to0)\equiv\hbar\omega_0=\frac{\hbar^2k^2}{2m^*_H}, \tag{6.9}$$

which can be calculated from the self-energy,

$$\frac{m_3}{m^*_H}=1+\lim_{k\to0+}\frac{2m_3}{\hbar^2k^2}\Sigma^{(3)}(k,\omega_0). \tag{6.10}$$

A particularly simple approximate form for the self-energy is the so-called ''uniform-limit approximation''[10] where $\beta^{(34)}_{\mathbf{k},\omega_0}(\mathbf{p})$ has the form[25]

$$\beta^{(34)}_{\mathbf{k},\omega_0}(\mathbf{p})=\frac{\hbar^2}{2m_3}\mathbf{k}\cdot\mathbf{p}\frac{S^{(34)}(p)}{S^{(44)}(p)}. \tag{6.11}$$

In this approximation, one obtains via equations (6.5) and (6.10) the ''unrenormalized effective mass'' derived by Owen.[42]

$$\left.\frac{m^*_H}{m_3}\right)_{un}=\frac{1}{1-I} \tag{6.12}$$

with

$$I=\frac{1}{2}\int\frac{d^2p}{(2\pi)^2\rho_4}\frac{[S^{(34)}(p)]^2}{S^{(44)}(p)}\frac{t_3(p)}{t_3(p)+\epsilon(p)}. \tag{6.13}$$

This simple form of the effective mass also results from a Green's function theory as will be discussed below.

In a slightly different approximation[25] one ignores the integral term in Eq. (6.7) and uses the effective mass approximation of Eq. (6.9). That leads to the ''renormalized effective mass''

$$\left.\frac{m^*_H}{m_3}\right)_{re}=1+I. \tag{6.14}$$

Results for the ''unrenormalized'' and ''renormalized'' effective masses together with the full solution of the integral equation (6.7) are shown in Table I. From the structure of Eq. (6.12) it is clear that one has a divergence when the correlations described by the self-energy correction (6.13) become too large. This divergence is removed in the ''renormalized'' version and also in the full calculation which is always between the ''unrenormalized'' and the ''renormalized'' result.

C. Fermi liquid effective mass

The hydrodynamic effective mass is a consequence of the interaction of a single ^{3}He atom with the host liquid at low energies. Further interesting effects arise from the interaction

TABLE I. The effective mass of the ^{3}He impurity in the low–concentration limit. The second column shows the ''unrenormalized'' effective mass (6.12), which is also obtained in the $G0W$-approximation. The third column shows the ''renormalized'' effective mass (6.14) and the last column the result with the full solution of the integral equation (6.7).

ρ [Å^{-2}]	Unren.	Ren.	Full
0.040	1.756	1.430	1.683
0.045	1.910	1.476	1.754
0.050	2.123	1.529	1.831
0.055	2.424	1.588	1.910
0.060	2.883	1.653	1.994
0.065	3.694	1.729	2.086

between pairs of ^{3}He atoms and the specific dynamics imposed on the ^{3}He component by the Pauli principle. The most obvious manifestations of interactions between the ^{3}He atoms are magnetic properties[43] and corrections to the hydrodynamic mass. The appropriate framework to discuss these effects is Landau's quasiparticle theory.[44]

The quasiparticle interaction normally contains a spin-independent and a spin-dependent part,

$$f^{\mathrm{var}}_{\mathbf{k}\sigma,\mathbf{k}'\sigma'} = f^{\mathrm{s}}_{\mathbf{k},\mathbf{k}'} + f^{\mathrm{a}}_{\mathbf{k},\mathbf{k}'}\,\boldsymbol{\sigma}\cdot\boldsymbol{\sigma}', \tag{6.15}$$

where the $\boldsymbol{\sigma}$'s are Pauli spin matrices. Since both wave vectors $\mathbf{k}$ and $\mathbf{k}'$ are on the Fermi surface, the quasiparticle interaction depends only on the angle between $\mathbf{k}$ and $\mathbf{k}'$. In two dimensions, $f^{\mathrm{s\,(a)}}_{\mathbf{k},\mathbf{k}'}$ is expanded in a Fourier series[45]

$$f^{\mathrm{s\,(a)}}_{\mathbf{k},\mathbf{k}'} = \sum_m f^{s(a)}_m \cos(m\phi), \quad \cos\phi = \hat{\mathbf{k}}\cdot\hat{\mathbf{k}}'. \tag{6.16}$$

The strength of the interaction relative to the kinetic energy is measured by the dimensionless quantities

$$F^{\mathrm{s\,(a)}}_m = N(0) f^{\mathrm{s\,(a)}}_m = \frac{\Omega m^*}{\pi\hbar^2} f^{\mathrm{s\,(a)}}_m, \tag{6.17}$$

where $N(0)$ is the density of states at the Fermi surface, and m^* is the effective mass. In first approximation, the quasiparticle interaction can be identified with the matrix elements of the energy-dependent effective interaction

$$\tilde{V}_{\mathrm{eff}\backslash}(q,\omega) = \tilde{V}^{(33)}_{\mathrm{p\text{-}h}}(q) + \sum_{\alpha\beta} \tilde{V}^{(3\alpha)}_{\mathrm{p\text{-}h}}(q)\chi^{(\alpha\beta)}(q,\omega)\tilde{V}^{(3\beta)}_{\mathrm{p\text{-}h}}(q) \tag{6.18}$$

taken at zero energy,

$$f_{\mathbf{k},\boldsymbol{\sigma},\mathbf{k}',\boldsymbol{\sigma}} = \langle \mathbf{k}\sigma,\mathbf{k}'\sigma' | \tilde{V}_{\mathrm{eff}}(\omega=0) | \mathbf{k}\sigma,\mathbf{k}'\sigma' - \mathbf{k}'\sigma',\mathbf{k}\sigma\rangle. \tag{6.19}$$

Quantities of primary interest are the effective mass and the magnetic response of the system.

An alternative way to calculate the effective mass, which will momentarily be seen to be more easily implemented in the present framework, is to calculate the single-particle spectrum $\hbar\omega(k)$ and to obtain the effective mass from

$$\frac{\hbar^2 k_F}{m^*} \equiv \frac{d}{dk}\hbar\omega(k)\bigg|_{k=k_F}. \tag{6.20}$$

The fermion generalization of the ''uniform-limit approximation'' (6.10) and (6.11) for the self-energy $\Sigma^{(3)}(k,\omega)$ is the $G0W$-approximation,[46,47]

$$\Sigma(k,\omega) = i\int \frac{d^2q\,d(\hbar\omega')}{(2\pi)^3\rho_3} G^{(0)}(|\mathbf{k}-\mathbf{q}|,\omega-\omega')\tilde{V}_{\mathrm{eff}\backslash}(q,\omega'), \tag{6.21}$$

where $\tilde{V}_{\mathrm{eff}\backslash}(q,\omega)$ has been defined in Eq. (6.18), and

$$G^{(0)}(k,\omega) = \frac{1-n_{\mathbf{k},\sigma}}{\hbar\omega - t_3(k) + i\eta} + \frac{n_{\mathbf{k},\sigma}}{\hbar\omega - t_3(k) - i\eta} \tag{6.22}$$

is the free single-particle Green's function of the ^{3}He impurity. Taking the single-impurity limit $n_{\mathbf{k},\sigma}=0$ recovers the ''unrenormalized'' effective mass mentioned above.[25]

The single-particle spectrum $\hbar\omega(k)$ is changed, from its single-impurity approximation (6.4) and (6.11), by two effects: One is the Fermi statistics, manifested by the occupation numbers $n_{\mathbf{k},\sigma}$ in the single-particle Green's function and in the (33) component of the density-density response function. The second effect is due to the presence of the concentration-fluctuation mode. This mode becomes, as shown above, soft as the spinodal concentration is approached from above. Such a mode softening is accompanied by a singularity of the effective interaction, leading to a singular effective mass. Because of this, the two-dimensional mixture is expected to display quite different effects than the three-dimensional analog: in three dimensions, the effective mass is always dominated by the hydrodynamic backflow, in other words by the coupling of the impurity motion to the *density fluctuations.* In two dimensions, this coupling can be overshadowed by the coupling to *concentration fluctuations.* We can still define a ''hydrodynamic mass'' at finite concentrations, which is obtained by keeping only the (44) component of the density-density response function in Eq. (6.18). This hydrodynamic mass should provide a smooth background, whereas the coupling to concentration fluctuations dominates as the concentration is lowered. However, in the mixture, the purely hydrodynamic effects caused by coupling-to-density fluctuations, and enhancement caused by the coupling-to-concentration fluctuations are hard to disentangle.

Equation (6.4) should be solved self-consistently; the effective mass at the Fermi momentum k_F can then be calculated from Eq. (6.20). We have simplified the numerical task by using an effective mass approximation $t_3^*(k) \equiv \hbar^2k^2/2m_3^*$ in the single-particle Green's function (6.22). This is appropriate when the spectrum is real and reasonably structureless. Since significant quasiparticle damping sets in only when the energy of the quasiparticle approaches that of the roton[41] we consider this approximation sufficient for our purposes.

The results shown in Fig. 20 are consistent with the above discussion: When only density fluctuations are retained, the

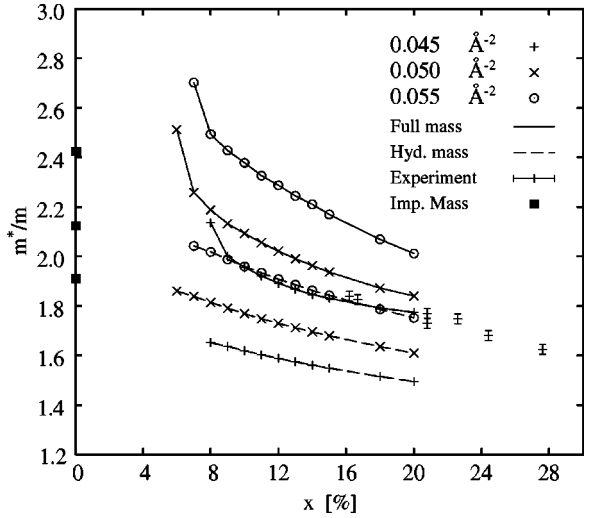

FIG. 20. The figure shows the effective mass ratio of the ^{3}He atom, for the three densities 0.045 Å^{-2} (+ symbols), 0.050 Å^{-2} (crosses), and 0.055 Å^{-2} (circles), as a function of concentration x. The dashed lines are results obtained by keeping the (44)–channel of the response function only, whereas the solid lines display the results of the calculation keeping both density- and concentration fluctuations. The square boxes at the left margin show the zero-concentration limit, Column 2. of Table I. The crosses with error bars are results extracted from the experimental data of Ref. 48 as described in the text.

effective mass is moderate and extrapolates with reasonable accuracy to the ''unrenormalized'' approximation in the zero-concentration limit that was obtained in a completely independent calculation. The concentration dependence is visible, but moderate. However, the corrections due to including concentration-fluctuations are, contrary to the three-dimensional case, *not* small; they display the expected divergence as the system approaches the instability point.

In order to compare with the experiments of Ref. 48, we must take into account that these were carried out on films with finite thickness adsorbed to a substrate. Only experiments on very thin films are suitable for comparison with our results: As the ^{4}He coverage is increased, the ^{3}He impurity atoms will start populating Andreév states in the surface, and the assumption of a two-dimensional mixture becomes invalid. This behavior can be seen experimentally in the fact that the effective mass first increases, and then decreases, with increasing coverage. The transition from a two-dimensional mixture to a system where the ^{3}He atoms populate Andreév states in the ^{4}He surface occurs[49] at an areal density of about 0.055 Å^{-2}, this density is quite resilient under changes of the substrate as long as its attaction is reasonably strong. Hence only data below that liquid coverage are suitable for comparison.

The experiments of Ref. 48 have been done at a constant ^{3}He areal density $\rho_3 = 0.019$ Å^{-2}, and were given in terms of the thickness $D(\rho) = \rho/\overline{\rho}_{\rm exp}$ of the ^{4}He film. ($\overline{\rho}_{\rm exp} = 0.021\,85$ Å^{-3} is the experimental equilibrium density of ^{4}He.) The concentration is obtained from this by

$$x = \frac{\rho_3}{\rho} = \frac{\rho_3}{\rho_3 + \rho_4}. \tag{6.23}$$

The resulting concentrations and total densities are—considering the fact that the two-dimensional model becomes physically questionable above $\rho = 0.055$ Å^{-2}—beyond the density where we have confidence in the two-dimensional model; hence much caution is needed for their interpretation.

The results of our calculations and a comparison with some of the data from Ref. 48 are shown in Fig. 20. As indicated above, the total densities for the experimental data range between 0.1 Å^{-2} (the lowest concentration of 16.2%) and 0.07 Å^{-2} (the highest concentration of 27.8%. One could shift the total densities somewhat by allowing for an inert solid layer, but that would increase the ^{3}He concentration to values of 50% and more.

D. Magnetic response

The magnetic response is determined by the change of the quasiparticle energy when an external magnetic field H is applied. The spin susceptibility χ_σ is related to the Landau parameter $F_0^{\rm a}$ by

$$\frac{\chi_{\sigma,0}}{\chi_\sigma} = \frac{m}{m^*}\left(1 + \frac{m^*}{\pi\hbar^2}\Omega f_0^{\rm a}\right) = \frac{m}{m^*}(1 + F_0^{\rm a}). \tag{6.24}$$

Since the effective interaction is provided by the ground-state calculation, we can directly calculate the Landau-parameter from Eq. (6.18)

$$\Omega f_0^{\rm a} = -\frac{1}{2\rho_3}\int \frac{d\theta}{2\pi}\tilde{V}_{\rm eff}(|\mathbf{k}_{\rm F} - \mathbf{k}'_{\rm F}|, 0). \tag{6.25}$$

As seen from Eq. (6.17), two effects contribute to the susceptibility. One is the density of states of the interacting Fermi gas at the Fermi surface, manifested in the effective mass m^* discussed in the previous section. The second is the quasiparticle interaction in the spin channel. To disentangle these two effects, we define an additional set of Landau parameters by replacing the effective mass by the bare mass in Eq. (6.17), i.e., $\overline{F}_m^{s(a)} = (m/m^*)F_m^{s(a)}$, where the $\overline{F}_0^{(a)}$ measures the strength of the spin-channel interaction (6.25) alone. The result is shown, as a function of concentration, in Fig. 21. At the spinodal point, the $\overline{F}_m^{s(a)}$ diverges just as the effective mass ratio; however, as the concentration is lowered, the rapid increase of the effective mass m^* is the dominant effect.

Finally, we show in Fig. 22 the total magnetic susceptibility of the two-dimensional mixture, as well as the susceptibility coming from the density of states alone, as a function of density and concentration. Clearly, the corrections from the Fermi liquid interaction are strong, and in fact change the qualitative behavior of the magnetic susceptibility as a function of concentration. The same comments apply that were made concerning the effective mass above. Some caution should be applied when comparing these results with experiments[50] since the two-dimensional model does not allow for a (partial) geometric separation between ^{3}He and ^{4}He through the population of Andreév states. To verify our results experimentally would take a different environment; a possibility for this will be discussed momentarily.

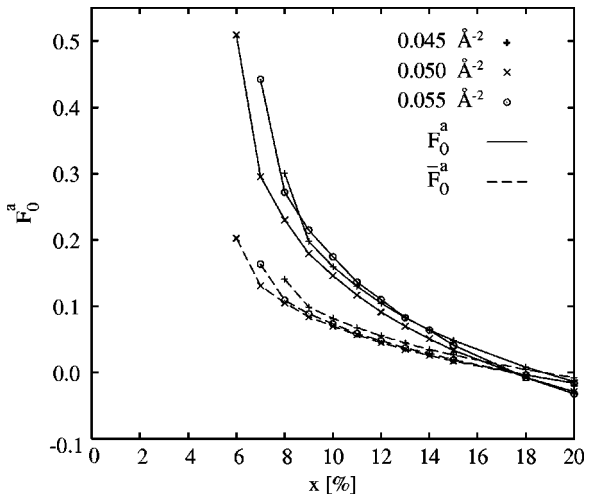

FIG. 21. The figure shows the Landau parameter F_0^a as a function of concentration at three different areal densities (crosses, and lines as marked in the figure). Also shown are the quantities $\overline{F_0^a}$ obtained by setting the effective mass equal to the bare mass.

VII. SUMMARY

We have, in this paper, examined the structure of ^{3}He-^{4}He mixtures in two dimensions. This field has been a very active one over the past two decades, mostly in connection with quantum-liquid mixture films.

The assumption of a purely two-dimensional geometry made in this paper is certainly an idealization. This approximation may be justifiable in strongly bound mixture films, for example on the first ^{4}He liquid layer on graphite[51] or on the hydrogen plated graphite.[52] In such systems, and assuming that the two-dimensional approximation is valid, a close analysis of the basic physics and model-independent simulation data hints towards the existence of a very interesting phase diagram: At low ^{3}He concentrations, typically below 2%, we have shown that (a) a mixture is energetically preferable over a phase-separated system, and (b) the mixture does not exist in an atomic form, but rather in the form of ^{3}He dimers within in the ^{4}He background (''Bashkin states.'') The existence of these states is caused by the long-wavelength properties of the phonon-mediated interaction as, for example, discussed by Bardeen *et al.*[24] It relies, in particular, on the specific many-body technique applied only in the sense that the technique is consistent enough to reflect the statements of Bardeen *et al.* Also, the energetic advantage of the mixture over the phase-separated system is based on the analysis of simulation data for ^{3}He and ^{4}He in two dimensions as well as a very conservative estimate on the inaccuracies introduced by the ''average-correlation approximation.''

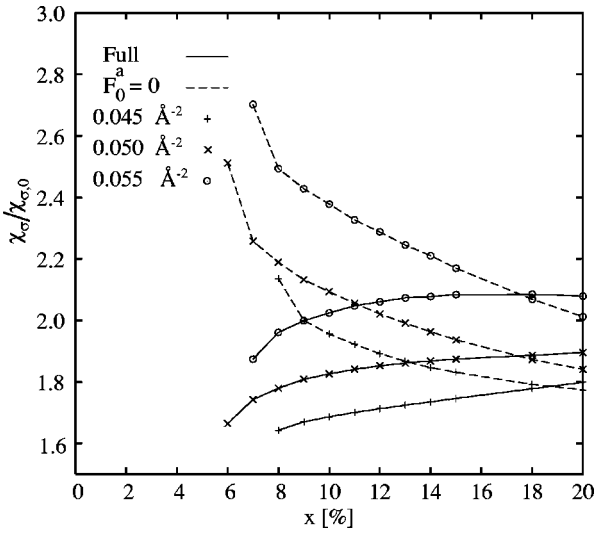

FIG. 22. The figure shows the magnetic susceptibility of the ^{3}He component for the three densities 0.045 Å^{-2}, 0.050 Å^{-2}, and 0.055 Å^{-2} as a function of concentration x (solid lines). Also shown are the susceptibilities obtained from the density of states alone, ignoring the spin-channel interaction altogether (dashed lines).

We have verified that our approximate (F)HNC-EL calculations are internally consistent and agree with simulation data whenever such comparisons were possible. Based on these calculations, we have shown that an atomic mixture may be stable against infinitesimal concentration fluctuations above a concentration of 2–3 %. This concentration approaches, however, the value where global energy comparisons would predict that the mixture phase separates. The whole rich scenario discussed here comes out as a consequence of the structure of our theory, in particular the optimization of the correlations that prevent the theory from predicting physically unstable situations. From the point of theory, this is yet another strong argument for optimization as compared with the use of parametrized correlation functions. None of the above physics was predicted in the work by Um *et al.* who have pursued, along with some technical simplifications, this path.

As noted above, the assumption of a rigorously two-dimensional geometry is an idealization, and it is time to discuss the most likely consequences of this in respect to both the ^{4}He background and the ^{3}He component. We have studied in Ref. 53 among others atomic ^{4}He monolayers on substrate potentials of varying strength, allowing for a full symmetry breaking in the direction perpendicular to the substrate. Expectedly, we found that the energy of the system is lowered when the particles have more freedom to move in the direction perpendicular to the surface. Such an energy lowering has been found even in the first liquid layer above the two solid layers on a rather strongly attractive graphite substrate where one should expect that the two-dimensional approximation is quite valid.

In an independent study of the binding of isolated pairs of helium atoms[54] we have, among others, clarified the reason for this. A pair of helium atoms is, independent of the species, most strongly bound if the width of the holding potential is comparable to the width of the pair potential. The increase in binding energy can be quite dramatic, ranging from a factor of 2 for ^{4}He dimers to over two orders of magnitude for ^{3}He dimers. Thus, we expect that the dimerization will be enhanced in a more realistic situation. On the other hand, we have shown above that rigorously two-dimensional mixtures are, at the high concentrations studied

in Ref. 48, unstable against phase separation. It is an open, and quite interesting problem, to see if and how the finite width of the film geometry, and the presence of an attractive substrate, can stabilize the atomic mixture.

A second difference between atomic monolayers and the two-dimensional approximation is the existence of surface excitations. In our studies of excitations of adsorbed films we found that, for low-coverage films with a surface coverage of less than 0.055 Å^{-2}, the lowest excitation is basically a two-dimensional sound wave with a speed that is comparable to the one of a two-dimensional liquid. However, as the coverage increases, beyond 0.055 Å^{-2}, the speed of this excitation drops rapidly, and the nature of the excitation turns from a two-dimensional phonon into a ripplon. This cross-over coverage of 0.055 Å^{-2} is quite resilient to the nature of the substrate potential. Since this excitation is much softer than the phonon, and since the main correction to the bare interaction between ^{3}He impurities is mediated by the excitations of the background, we should expect a further enhancement of the attraction between the ^{3}He impurities.[55,56] Note, in this connection, that the speed of sound appears in the denominator of the longest−ranged part of the induced interaction (4.12).

In conclusion, we have highlighted here a scenario of the structure of quantum-liquid mixture films that appears much richer than anticipated. We believe that a very careful analysis of both theoretical predictions and experimental data is called for to possibly detect the existence of ^{3}He dimers, to see, in the more realistic situation of atomic monolayers the consequences of ripplon coupling, and finally to study the nature of phase-separated mixture films where the ^{3}He atoms reside not within, but on top, of a helium film. In conclusion, we also mention a possibility to generate quasi-two-dimensional ^{3}He-^{4}He mixtures that have no free surface: Hectorite is a silicate that consists of regular quasi-two-dimensional layers of about 9.6-Å thickness and an open spacing of 17–20 Å in between. These gaps can be filled with liquid ^{4}He; the first experiments on this confined quantum liquid were carried out by Wada and co-workers.[57,58] Preliminary calculations[59] indicate that ^{3}He impurities, when brought into a hectorite gap filled with ^{4}He, are quite well localized in the middle of a gap and form indeed a practically two-dimensional Fermi liquid with no coupling to surface states.

ACKNOWLEDGMENTS

The work was supported, in part, by the Austrian Science Fund (FWF) under project No. P12832-TPH (E.K.), and the Academy of Finland under Project No. 163358 (M.S.). We would like to thank V. Apaja, J. Boronat, M. D. Miller, and J. Saunders for helpful discussions.

[1] R. B. Hallock, in *Progress in Low Temperature Physics* (North-Holland, Amsterdam, 1995), Vol. XIV, Chap. 5, pp. 321–443.
[2] R. B. Hallock, Phys. Today **51** (6), 30 (1998).
[3] M. Dann, J. Nyèki, B. P. Cowan, and J. Saunders, Phys. Rev. Lett. **82**, 4030 (1999).
[4] M. D. Miller, Phys. Rev. B **17**, 1139 (1978).
[5] E. Krotscheck, J. Paaso, M. Saarela, and K. Schörkhuber, Phys. Rev. Lett. **85**, 2344 (2000).
[6] E. Krotscheck and M. Saarela, Phys. Rep. **232**, 1 (1993).
[7] R. de Bruyn Ouboter and C. N. Yang, Physica B & C **144**, 127 (1986).
[8] R. A. Aziz, V. P. S. Nain, J. C. Carley, W. J. Taylor, and G. T. McConville, J. Chem. Phys. **70**, 4330 (1979).
[9] R. A. Aziz, F. R. W. McCourt, and C. C. K. Wong, Mol. Phys. **61**, 1487 (1987).
[10] E. Feenberg, *Theory of Quantum Fluids* (Academic, New York, 1969).
[11] C. E. Campbell, in *Progress in Liquid Physics*, edited by C. A. Croxton (Wiley, London, 1977), Chap. 6, pp. 213–308.
[12] C. E. Campbell and E. Feenberg, Phys. Rev. **188**, 396 (1969).
[13] C. E. Campbell, Phys. Lett. A **44**, 471 (1973).
[14] E. Krotscheck, Phys. Rev. B **33**, 3158 (1986).
[15] E. Krotscheck and M. L. Ristig, Phys. Lett. A **48**, 17 (1974).
[16] E. Krotscheck, J. Low Temp. Phys. **27**, 199 (1977).
[17] E. Krotscheck, J. Low Temp. Phys. **119**, 103 (2000).
[18] G. Ripka, Phys. Rep. **56**, 1 (1979).
[19] R. F. Bishop and K. H. Lührmann, Phys. Rev. B **26**, 5523 (1982).
[20] J. W. Clark, in *Progress in Particle and Nuclear Physics*, edited by D. H. Wilkinson (Pergamon Press, Oxford, 1979), Vol. 2, pp. 89–199.
[21] E. Krotscheck and J. W. Clark, Nucl. Phys. A **328**, 73 (1979).
[22] E. Krotscheck, Phys. Rev. A **26**, 3536 (1982).
[23] D. Pines and P. Nozieres, *The Theory of Quantum Liquids*, (Benjamin, New York, 1966), Vol. I.
[24] J. Bardeen, G. Baym, and D. Pines, Phys. Rev. **156**, 207 (1967).
[25] M. Saarela and E. Krotscheck, J. Low Temp. Phys. **90**, 415 (1993).
[26] J. C. Owen, Phys. Rev. Lett. **47**, 586 (1981).
[27] A. D. Jackson, A. Lande, and R. A. Smith, Phys. Rep. **86**, 55 (1982).
[28] A. D. Jackson, A. Lande, and R. A. Smith, Phys. Rev. Lett. **54**, 1469 (1985).
[29] E. Krotscheck, A. D. Jackson, and R. A. Smith, Phys. Rev. A **33**, 3535 (1986).
[30] A. D. Jackson, Annu. Rev. Nucl. Part. Sci. **33**, 105 (1983).
[31] E. P. Bashkin, Zh. Éksp. Teor. Fiz. **78**, 360 (1980) [Sov. Phys. JETP **51**, 181 (1980)].
[32] K. Langanke, D. Lokas, H.-M. Müller, S. Schramm, and S. E. Koonin, Z. Phys. A **339**, 419 (1991).
[33] H.-M. Müller and K. Langanke, Phys. Rev. C **49**, 524 (1996).
[34] S. Giorgini, J. Boronat, and J. Casulleras, Phys. Rev. B **54**, 6099 (1996).
[35] J. Boronat (private communication).
[36] G. Baym, Phys. Rev. Lett. **17**, 952 (1966).
[37] J. Boronat, A. Fabrocini, and A. Polls, Phys. Rev. B **39**, 2700 (1989).

[38] C. Um, J. Kahng, and T. F. George, J. Low Temp. Phys. **112**, 399 (1998).
[39] M. Saarela, Phys. Rev. B **33**, 4596 (1986).
[40] C. C. Chang and C. E. Campbell, Phys. Rev. B **15**, 4238 (1977).
[41] E. Krotscheck, J. Paaso, M. Saarela, K. Schörkhuber, and R. Zillich, Phys. Rev. B **58**, 12 282 (1998).
[42] J. C. Owen, Phys. Rev. B **23**, 5815 (1981).
[43] E. P. Bashkin and A. E. Meyerovich, Adv. Phys. **30**, 1 (1981).
[44] L. D. Landau and I. Pomeranchuk, *On the Motion of Foreign Particles in Helium II* (Gordon and Breach, New York, 1967), pp. 469–470; Dokl. Akad. Nauk (SSSR) **59**, 669 (1948) [Sov. Phys. Dokl. **59**, 669 (1948)].
[45] S. M. Havens-Sacco and A. Widom, J. Low Temp. Phys. **40**, 357 (1980).
[46] L. Hedin, Phys. Rev. A **139**, 796 (1965).
[47] T. M. Rice, Ann. Phys. (N.Y.) **31**, 100 (1965).
[48] X. Wang and F. M. Gasparini, Phys. Rev. B **38**, 11 245 (1988).
[49] B. E. Clements, E. Krotscheck, and M. Saarela, Phys. Rev. B **55**, 5959 (1997).
[50] D. T. Sprague, N. Alikacem, P. A. Sheldon, and R. B. Hallock, J. Low Temp. Phys. **89**, 605 (1992).
[51] D. T. Sprague, N. Alikacem, P. A. Sheldon, and R. B. Hallock, Phys. Rev. Lett. **72**, 384 (1994).
[52] R. C. Ramos and O. E. Vilches, J. Low Temp. Phys. **113**, 981 (1998).
[53] B. E. Clements, J. L. Epstein, E. Krotscheck, and M. Saarela, Phys. Rev. B **48**, 7450 (1993).
[54] S. Kilić, E. Krotscheck, and L. Vranješ, J. Low Temp. Phys. **119**, 715 (2000).
[55] R. W. Anderson and M. D. Miller, in *Recent Progress in Many Body Theories*, edited by E. Schachinger, H. Mitter, and H. Sorrmann (Plenum, New York, 1995), Vol. 4, pp. 79–84.
[56] R. H. Anderson, M. D. Miller, and R. B. Hallock, Phys. Rev. B **59**, 3345 (1999).
[57] N. Wada, A. Inoue, H. Yano, and K. Torii, Phys. Rev. B **52**, 1167 (1996).
[58] M. Hieda, M. Suzuki, K. Torii, H. Yano, and N. Wada, Physica B **263-264**, 370 (1999).
[59] V. Apaja and E. Krotscheck, J. Low Temp. Phys. (to be published).